UNIVERSITY OF CALIFORNIA, SAN DIEGO

# Design of a Bioabsorbable Cardiopulmonary Shunt Cuff to Improve Outcomes of Blalock-Taussig Shunt Palliative Procedures

A Thesis submitted in partial satisfaction of the requirements for the degree Master of Science

in

Engineering Sciences (Mechanical Engineering)

by

Edward Aminov

Committee in charge:

Professor James Friend, Chair
Professor Juan Carlos Del Alamo
Professor Vishal Nigam

2017

The Thesis of Edward Aminov is approved and it is acceptable in quality and form for publication on microfilm and electronically:

---

---

---

Chair

University of California, San Diego

2017

# Table of Contents

# List of Figures

# List of Tables

THESIS ABSTRACT

Design of a Bioabsorbable Cardiopulmonary Shunt Cuff to Improve Outcomes of Blalock-Taussig Shunt Palliative Procedures

by

Edward Aminov

Master of Sciences in Engineering Sciences (Mechanical Engineering)

University of California, San Diego, 2017

Professor James Friend, Chair

Biodegradable polymers have been commonly implemented in controlled drug release, tissue engineering scaffolds, and short term prosthesis. The engineering of these biomaterials for their specific applications is crucial for the control of their mechanical and dissolution properties. The proper optimization of polycaprolactone for medical use requires development of a robust fabrication technique, analysis of mechanical and dissolution properties in a specific environment, and analysis of diffusion through the material. The thesis presents a novel technique for fabrication of complex geometry structures with polycaprolactone which allows for varying layers of porosity within the structure. Polycaprolactone sheets of 125 µm, 250 µm,

and 500 µm are fabricated and molded to create the complex elliptical geometry of the shunt cuff. The research further studies the effects of cyclic loading on the dissolution of porous polycaprolatone, revealing drastic decrease in dissolution time as well an altered dissolution profile under cyclic loading. A model for the effect of pore diameter, porosity, and section thickness on blood flow rate through the porous material due to dynamic blood pressure is developed. The fabrication technique and the dissolution properties of polycaprolactone can be engineered to create a bioabsorbable shunt cuff that satisfies the needed dissolution and strength properties required for application in a shunt cuff.

# 1 Introduction

Congenital heart defects—abnormal developments of the heart and major blood vessels—are the most common birth abnormalities in the United States, annually affecting 35,000 infants.[1] These defects result in circulation of poorly oxygenated blood throughout, leading to organ failure. Annually, 1,300 infants undergo palliative surgery which uses a pliable Gore-Tex tube as a shunt between an infant's systemic arteries and pulmonary artery to move blood to the lungs for re-oxygenation. The palliative surgery is required to maintain the required blood flow needs until a reparative surgery can be performed 6 months after birth. Improper sizing of the shunt[2] has consistently led to a 15%-25% mortality/morbidity rate since the shunts introduction in 1944. A shunt that is too small leads to low oxygen levels, known as cyanosis, while a shunt that is too large increases blood acidity, known as acidosis. Currently, infants are forced to undergo multiple surgeries to increase the size of the shunt as the infant's size and blood flow needs double in the first six months. Further, palliative procedure can cost up to $350,000 per infant annually, consequently leading to an economic burden of up to $187 million for U.S. patients combined.[4] The underpinning problem is the inability of the shunt to maintain the blood flow needs of a growing infant, leading to death/morbidity due to improper blood oxygenation, or frequent surgical intervention. The objective of the project is to create a shunt designed to adapt to the needs of a growing infant, eliminate the need for multiple surgical procedures, and accommodate somatic growth. The rationale is to avoid the poor outcomes of fixed size shunts through improving mortality and morbidity and decreasing costs. The hypothesis is that the dissolution properties of the bioabsorbable cuff will allow the shunt to grow in inner diameter over time in concert with the growth of the infant's blood flow needs. The cuff will be engineered to change in shape through dissolution in a manner such that it "grows with the infant" with minimal surgical

intervention. When first implanted, the shunt will have a constricted internal cross-sectional area that will increase in size as the cuff material is reabsorbed by the blood in a gradual, controlled, and reproducible fashion.

## 1.1 Congenital Heart Defects

Congenital heart defects (CHD) are characterized as imperfections of the heart present at birth which negatively influence the ability of the heart to properly function.[5] These defects can influence the proper circulation of blood throughout the body, as well as cause mixing of oxygenated and deoxygenated blood, leading to improper concentrations of oxygen delivered to organs. Affected infants may exhibit blue lips and nails, have difficulty breathing, and exhibit exhaustion while feeding. The defects are usually detected with a fetal echo-cardiogram before birth or diagnosed by a physician post-birth once the symptoms are noticed.[5]

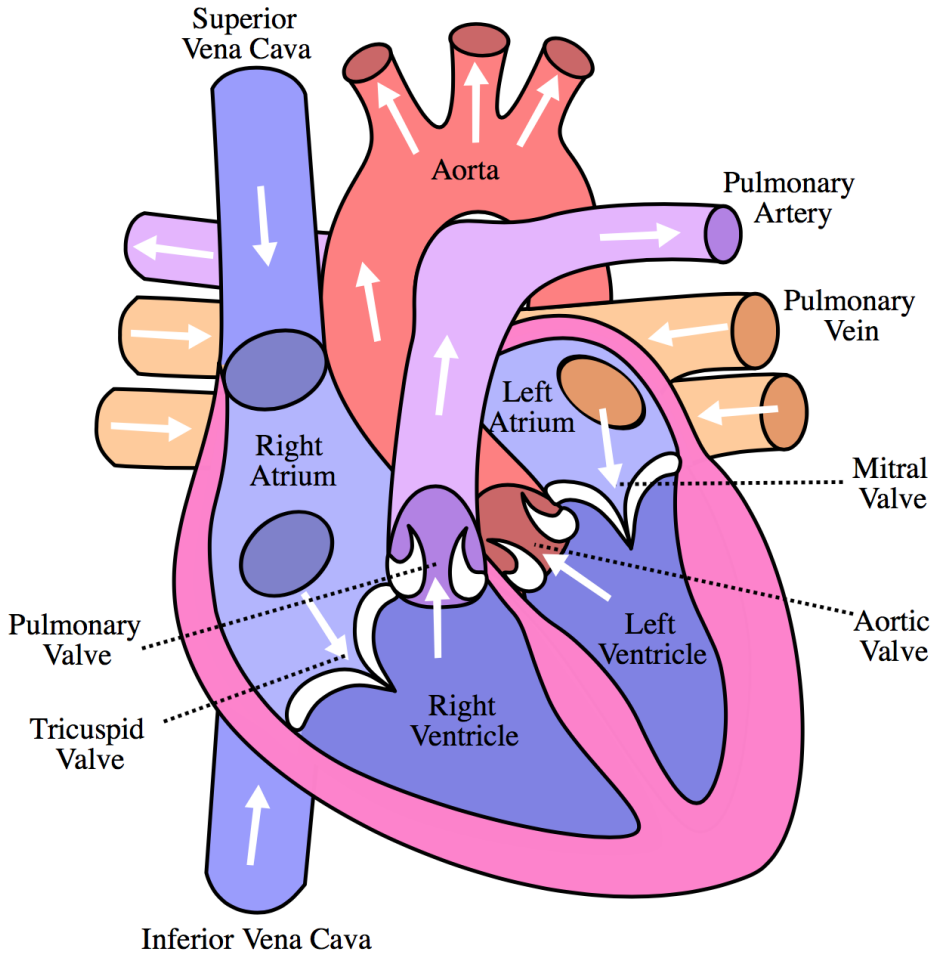


Figure 1: *A representation of the heart to understand the anatomy of congenital heart defects outlined below.*[6]

Examples of a CHD's are Atrial Septal Defects, in which the organism fails to close the cavity in the septum that divides the left and right atrium. While majority of the cavities heal early on after birth, some remain open and cause the mixing of the deoxygenated blood in the right atrium with oxygenated blood in the left atrium. Close to 2000 infants are born in the U.S. yearly with Atrial Septal Defects.[5] Coarctation of the aorta is another CHD, occurring in 4 out of 10,000 infants, in which the infant is born with an aorta that is narrow. The decrease in diameter of the aorta leads to higher resistance for the blood flow, forcing the left ventricle to pump with higher force and weakening the heart muscles. The condition leads to high blood pressure in the upper extremity, and low blood pressure in the lower extremities which is insufficient to supply organs.[5] One of the most serious examples of CHD is tetralogy of fallout, annually occurring in 1660 infants in the U.S., in which a total of four defects occur; a narrow pulmonary artery and valve, a larger aortic valve that opens from the left and right ventricles, a hole in between the left and right ventricles, and a thicker wall in the lower right chamber of the heart. These symptoms combine to cause cyanosis—blue baby syndrome— due to the low concentration of oxygen in the blood.[5] The prevalence of CHD has been on the rise since the 1930's. In the early part of the decade less than 1 per 1,000 live births were found to have congenital heart defects while in the last 15 years that number rose to approximately 9 per 1,000 live births.

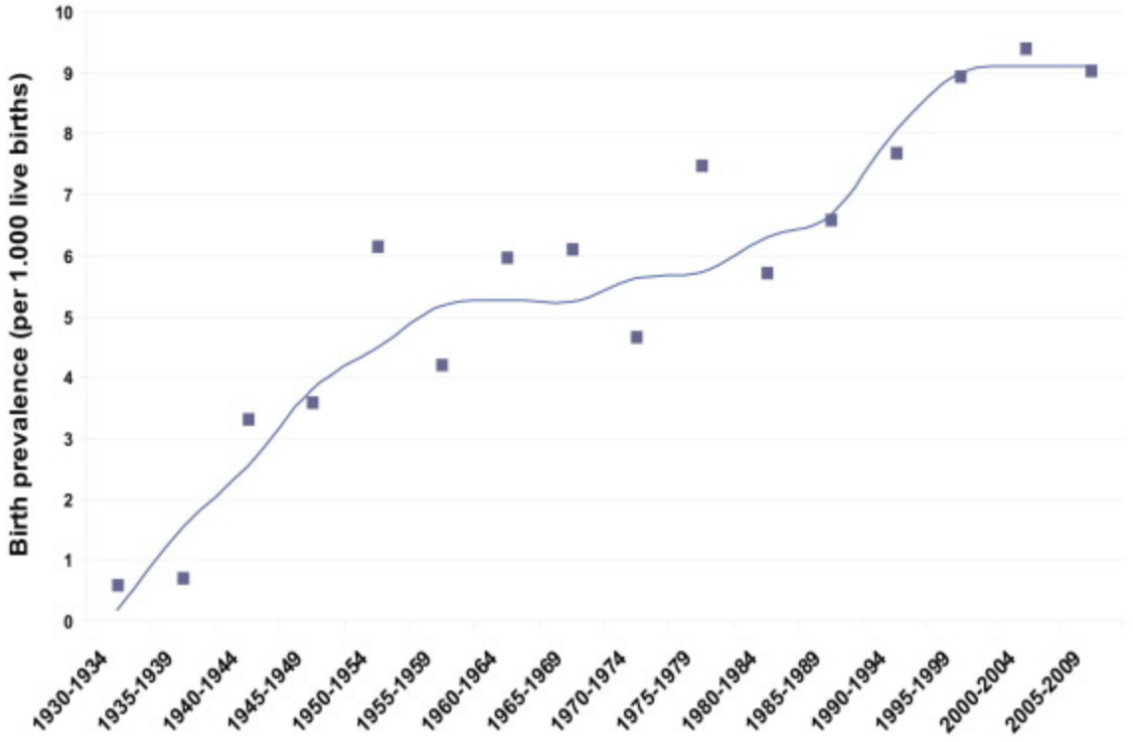


Figure 2: *Prevalence of CHD worldwide. A consistent and gradual rise is observed until 2000, after which the rate remains constant.*[8]

The rise in CHD over the years amounted to 1.35 million CHD births annually worldwide, defining it as a major public health issue.[8] As the prevalence increases, the treatment methods need to change to best mitigate the disabilities of CHD and significantly prolong and improve the lives of affected infants.

## 1.2 Current Treatment

The treatment of CHD is heavily dependent on the type of condition and its severity. In most cases, the defects heal naturally. Catheters may be used to treat conditions such as atrial septal defects in which a device that is attached to the catheter is deployed to cover the hole between the atriums.[9] In more serious cases, such as damaged valves or poor formation and location of arteries in the heart, the

physician will perform open heart surgery.[9] In these more complex cases, a palliative procedure is often required. A palliative procedure allows the infant to survive approximately six months after birth until the heart is developed enough for reparative surgery to be performed. The most common reparative surgery , discussed in more detail in the next section, is the Blalock-Taussig procedure.

### 1.2.1 Blalock-Taussig Shunt

A Blalock-Taussig (BT) shunt is a connection of a pulmonary and systemic artery with a tubular conduit that allows redirection of blood towards the lungs.[10] The procedure was first performed in 1944 on a 15 month old infant suffering from a CHD and has been widely applied for palliative surgery ever since. In most cases the shunt is connected between the subclavian artery and pulmonary artery. The purpose of the shunt is to satisfy the blood flow needs of the infant for the first six months until complete reparative surgery, anatomical reconfiguration, can be performed.[10] During this time, the shunt serves to direct a higher volume of blood towards the lungs for reoxygenation to decrease cyanosis. Over the years it has been concluded that even with the defect present and still causing intermixing of blood, the higher throughput into the lungs leads to a higher systemic oxygen saturation.[10] The modified BT shunt was introduced in 1962 to improve the classic procedure by reducing damage that may be caused to the pulmonary artery. The modified procedure also allows access to perform surgery on the same side as the aortic arch.[10] The modified procedure, which is the most commonly used for palliation today, uses Gore-Tex instead of Dacron to make up the tubular conduit connection.

### 1.2.2 Gore-Tex Properties

Gore-Tex has been the standard material used for the mBT procedures due to its desirable properties. Gore-Tex shunts are made up of expanded

polytetrafluoroethylene (ePTFE). Gore-Tex is known for its flexibility that allows its appending to arteries and synchronization with pulsatile blood pressure. The material has smaller pores, approximately 14 million per square meter,[12]than Dacron which limits the ability of cells to attach and grow in the material while allowing fibroblasts to form stronger bonds at the ends where it is connected to arteries.[10] For CHD applications the Gore-Tex used is in between 3.5 mm- 5 mm with a wall thickness of 395 µm.[13] The density was determined to be 3360 $\mathrm{kg\,m^{-3}}$ and an elastic stiffness of 40.6 MPa[13].[14]

## 1.3 Unmet Need

A range of factors contribute to the success of the palliative procedure. The accelerated growth of an infant within the initial six months of life leads to constantly changing blood flow needs. The variability between surgeons in properly sizing the initial shunt creates a variability in outcomes for the procedure. Lastly, the combination of growth and variability leads to an increased rate of surgical intervention, endangering the infant and driving up costs.

### 1.3.1 Procedure Cost

Costs are a deciding factor for many innovations in the medical field. The four factors contributing to the cost of the mBT procedure are initial hospitalization, cardiac catheterization, additional surgery, and stay in the intensive care unit (ICU). The initial hospitalization costs an average of $200,000 and currently cannot be prevented without preventing the defect in the first place.[15] Cardiac catheterization is caused by the need to expand the size of the Gore-Tex as the infant doubles in size, costing $25,000-$75,000.[16] Instances in which cardiac catheterization is not enough, surgeons must perform additional open heart surgery, costing approximately $60,000.[17] After each surgery the infant recovers in the ICU

which costs an additional $2,000 per day.[18] The total cost is $295,000-$345,000 per patient, and $122 million-$187 million annually for all patients. The high cost create a need to limit or eliminate the need for cardiac catheterization, additional surgery, and stay in the ICU to make the procedure less resource intensive.

### 1.3.2 Variability in Initial Sizing

It is of utmost importance to maintain the proper size of the shunt for the purpose of controlling oxygenated blood flow throughout the body.[19] The Gore-Tex is initially constricted to prevent acidosis that is associated with a shunt too large which creates a concentration of blood oxygen above normal. The constriction is performed via banding and partially clipping the shunt. Due to the dependence of clipping and banding on the surgeon, the location along the length, and the diameter of the shunt used, the process has been of poor precision[20].[21] A constriction that is initially too small may lead to cyanosis due to lack of oxygen or require the next step of palliation at an earlier time when the infant is not physiologically prepared.

### 1.3.3 Frequency of Surgical Intervention/Loss of Fit

The variability in initial sizing combined with the accelerated growth rate of the infant throughout the first six months leads to additional surgical intervention throughout the healing process. The surgeon can regulate the flow to the lungs through the resistance of the Gore-Tex. The resistance is directly dependent on length and diameter. Length is a poor controlling mechanism due to the possible kinking of the shunt if it is too long, which may lead to formation of blood clots and a higher resistance than desired. Additionally, changing length would require re-stitching of the shunt to the walls of the systemic and pulmonary arteries. Adjusting the diameter can also be done by releasing the pressure of clipping and banding,[19] once again introducing the issue of variability as well as the need for

additional surgery. At best, cardiac catheterization can be used for expanding the shunt, but often open heart surgery is required once more. Aside from the physiological shock of frequent surgery, the intervention leads to the morbidity and mortality associated with mBT palliation.[19]

#### 1.3.4 Blood Flow Monitoring

A common reason for failing of the mBT shunt is thrombosis. The constriction geometry and kinking in the shunt may lead to recirculating patterns of flow within the shunt which causes the formation of blood clots.[22] These clots are usually found once the child becomes cyanotic, or at the periodic echo-gram performed by a physician. To prevent delayed discovery of clotting there is a need to monitor blood flow through the cuff and detect changes in flow rate prior to development of symptoms.

### 1.4 Proposed Solution

The proposed solution needs to address the procedure cost, variability in sizing, frequent surgical intervention, and ability to prevent or monitor thrombosis. All four needs can be addressed through the design and fabrication of a cuff that will surround the shunt and gradually release its constriction over time. The cuff will be designed to gradually change in shape through controlled dissolution of its bioabsorbable matrix such that it "grows with the infant" with no surgical intervention. The interaction of the cuff and shunt is presented below.


Figure 3: *The interface between the innovative cuff and the Gore-Tex shunt.The shunt is constricted by the inner bioabsorbable component of the cuff (green). The cuff outer component (red) remains rigid and provides structure for the shunt-cuff complex.*

As the inner cuff material dissolves, the diameter and cross sectional area decrease, leading to an decrease in flow resistance and higher pulmonary flow rate. The higher pulmonary flow rate increases the concentration of oxygenated blood as needed by the growing infant. The application of the cuff is shown below.

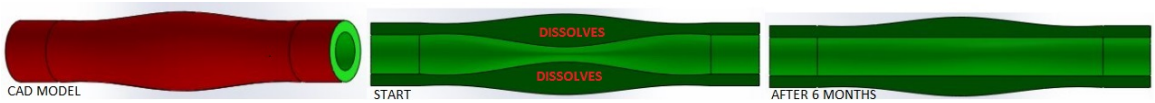


Figure 4: *Model of exterior of the cuff with an elliptical cross section. The outer layer will have the highest dissolution time to provide structural support for the shunt as the inner material dissolves (left). Interior of the cuff at the initial stage. The biodegradable material (green) constricts the blood flow through the shunt by decreasing the area. As the material is degraded, the area expands, gradually increasing blood flow through the shunt with the needs of the infant (center). Interior of the cuff at the final stage. The dissolution is complete and the shunt is returned to original size. At this stage the blood flow is identical to the blood flow through a normal mBT shunt needed for a six month old infant (right).*

The elliptical constriction is of critical importance to the design of the cuff as it allows for a decrease in cross sectional area while conserving the circumference, preventing the kinking of the shunt.

Design Requirement

- A safe, controlled increase in the shunt inner area from $7.07\,\mathrm{mm}^2$ (equivalent to

circular diameter of 3.0 mm) to 12.57 $mm^2$ (equivalent to circular diameter of 4.0 mm) over a period of 6 months. This represents a 78% increase in cross-sectional area and an estimated doubling of the blood flow rate increase through the shunt, taking into account the growth of the congenitally defective heart and surrounding vascular structure over this time.

- Maintenance of the constriction area despite the cardiac cycle, manipulation by the surgeon, and movement without anticipated injury to the patient post-implantation.

- Avoidance of kinking, wrinkling, or pinching of the shunt within that could lead to flow recirculation or patterns of blood stasis, and in turn could increase risk of thrombosis. By using an elliptical constriction, it is possible to both reduce the cross-sectional area of the shunt and avoid significant changes in the perimeter of the shunt, thereby avoiding the risk of wrinkling and consequent thrombosis. We have selected a 5.8 mm by 1.6 mm elliptical cuff for the constriction, which has the same cross sectional area as a 3.0 mm shunt while having the same perimeter as 4.0 mm shunt in order to control shunt flow without increasing the risk of thrombosis (see Fig.4). As the cuff dissolves, the effective shunt flow will go from the equivalent of a 3.0 mm shunt to that of a 4.0 mm shunt. The perimeter of the shunt remains nearly constant throughout.

### 1.5 Biomaterials

For the purpose of controlled dissolution in the human body biomaterials will be applied. More specifically, Polycaprolactone(PCL) and poly-(lactide-co-glyco-lide)(PLGA) will be engineered to fit the dissolution time and mechanical strength required for the mBT procedure.

### 1.5.1 Common Biomaterials and Their Applications

Biodegradable polymers have been commonly implemented in controlled drug release, tissue engineering scaffolds, short term prostheses, and more recently even degrading stents. Biodegradable materials can be characterized into synthetic and natural groups. Further, the materials can be grouped based on their dissolution method. Enzymatically degrading polymers, which are commonly found among natural polymers, require the presence of specific enzymes to cleave the polymer chains. Degradation rate can be well controlled through polymer chain chemical manipulations. Even though natural polymers best mimic physiological properties by offering receptors for cell communication, cell integration, and remodeling by cells, the high bioactivity of the polymers leads to strong immune responses.[24] Additionally, the reliance on enzymes for degradation leads to a high variation in dissolution rates in different regions of the body.[24] Synthetic polymers, which commonly undergo hydrolytic degradation, rely on hydrolysis as the main form of polymer breakage. In hydrolysis a water molecule is introduced into the polymer chain to break up that chain (Fig.5). The reliance on water for degradation allows synthetic polymers to maintain similar dissolution rates throughout the body.

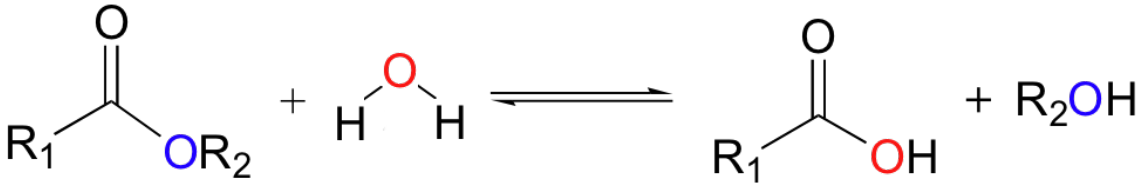


Figure 5: *Generalized hydrolysis for organic molecules. The water molecule breaks up the chain to one of the functional groups by introducing a hydroxide group on the original polymer chain and the dis-attached polymer group.*[23]

Additionally, the lack of natural receptors for cells limit the biological activity of synthetic polymers and reduce patient immune response.[24] The common functional groups found in hydrolytically include urethanes, carbonates, anhydrides,

and esters.[24] Poly($\alpha$-ester)s are the most frequently used hydrolytically degrading materials. They exhibit thermoplastic behavior which allows for fabrication at higher temperatures and maintenance of strong mechanical properties at body temperature. The polymer chains in poly($\alpha$-ester)s are shorter compared to other biodegradable polymers which reduces the in-vivo dissolution times to applicable ranges. Three subgroups of poly($\alpha$-ester)s: glycolides, lactides, and caprolactones are best suited for implementation in the bioabsorbable cuff. Glycolides,lactides, and caprolactones can be chemically combined to form co-polymers of different ratios through which dissolution time can be controlled. Additionally, all three members dissolve into either lactic or glycolic acid in-vivo;[24] both of which are found in the human metabolic pathway and can be safely excreted through urine. Table 1 below summarizes the most studied properties of the biomaterials that will be implemented for the bioabsorbable cuff.

Table 1: *The dissolution and mechanical properties of the most common poly(alpha-ester)s are presented in the above table. Poly(lactic-co-glycolic) acid (PLGA) of different lactide:glycolide ratios allows for a better discretized range of dissolution times.*[24–27]

| **Material** | Polycaprolactone | Polylactide | Polyglycolide | PLGA 85/15 | PLGA 75/25 | PLGA 65/35 | PLGA 50/50 |
|---|---|---|---|---|---|---|---|
| **Molecular Weight (kg/mol)** | 14-80 | 128-152 | 30 | 50-75 | 50-75 | 50-75 | 50-75 |
| **Melting (C)** | 60 | 175 | 200 | 200 | 200 | 200 | 200 |
| **Glass Transition (C)** | 60 | 60 | 40 | 60 | 50-55 | 45-55 | 41-55 |
| **Dissolution Time** | 2-3 years | 12-16 months | 12 months-6 years | 5-6 months | 4-5 months | 3-4 months | 1-2 months |
| **Elastic Modulus (Gpa)** | 1.2 | 1.9-4.8 | 12.5 | 2 | 2 | 2 | 2 |
| **Tensile Strength (Mpa)** | 23 | 50 | | 41-55 | 41-55 | 41-55 | 41-55 |
| **Yield Strength (Mpa)** | 8.2-10.1 | | | 3.5 | | | |
| **Molecular Structure** | 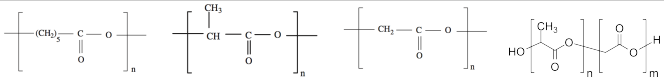 | | | | | | |

### 1.5.2 Methods of Biomaterial Degradation

Understanding the mechanisms by which biodegradable polymers erode and the environmental conditions that affect their degradation rates is important in successfully modeling their dissolution. For the purpose of this study, polymers

undergoing hydrolysis will be the main concentration. The most significant factors affecting hydrolysis of these biodegradable polymers are chemical bonds, environmental pH, co-polymerization, and water uptake. The chemical bond connecting monomers affects the rate of hydrolysis. The charge and the size of the functional group alter the ability of water to insert itself between the monomers. In some cases, changes a hydrogen atom with a chlorine can increase the reaction rate by 18 orders of magnitude.[28] Polymers with less bulky functional groups exhibit higher dissolution rates due to decreased steric hindrance. The pH surrounding the micro-environment of the reaction can increase the degradation rate of a polymer depending on whether the polymer is acid or base catalyzed.[28] Auto-catalysis, in which the degradation of a polymer serves as positive feedback to increase reaction rate, is especially important in determining the reaction rate. Specifically for PLGA, the degradation leads to formation of carboxylic acid which decreases the pH of the environment and increases reaction rate if the acid catalyzed polymer.[28] Mixing multiple polymers into a single chain leads to different molecular weights and access to functional groups, leading to a change of reaction rates and dissolution times as observed among different PLGA ratios in Table 1. Hydrophobicity properties of the polymer influence degradation rates by controlling the proximity and concentration of water molecules relative to polymer chains. Hydrophilic polymers tend to allow water to penetrate between polymer chains and increase reaction sites available.[28] The breakdown of polymers occurs in two steps, degradation and erosion. Initially the polymer undergoes degradation,a chemical reaction in which it is broken into smaller chains. These smaller chains are then subjected to diffusion, and are dis-attached from the original body, known as erosion. Degradation leads to a decrease in molecular weight and erosion leads to a decrease in total mass.[28] Additionally, each polymer exhibits a mix of surface and bulk erosion properties. In surface erosion, the reaction occurs on the outer surface of the material structure,

maintaining the geometry of the material and simply scaling it to a smaller size. In bulk erosion, the degrading molecule penetrates the structure of the polymer and degradation occurs on the surface and within. The process is illustrated below.

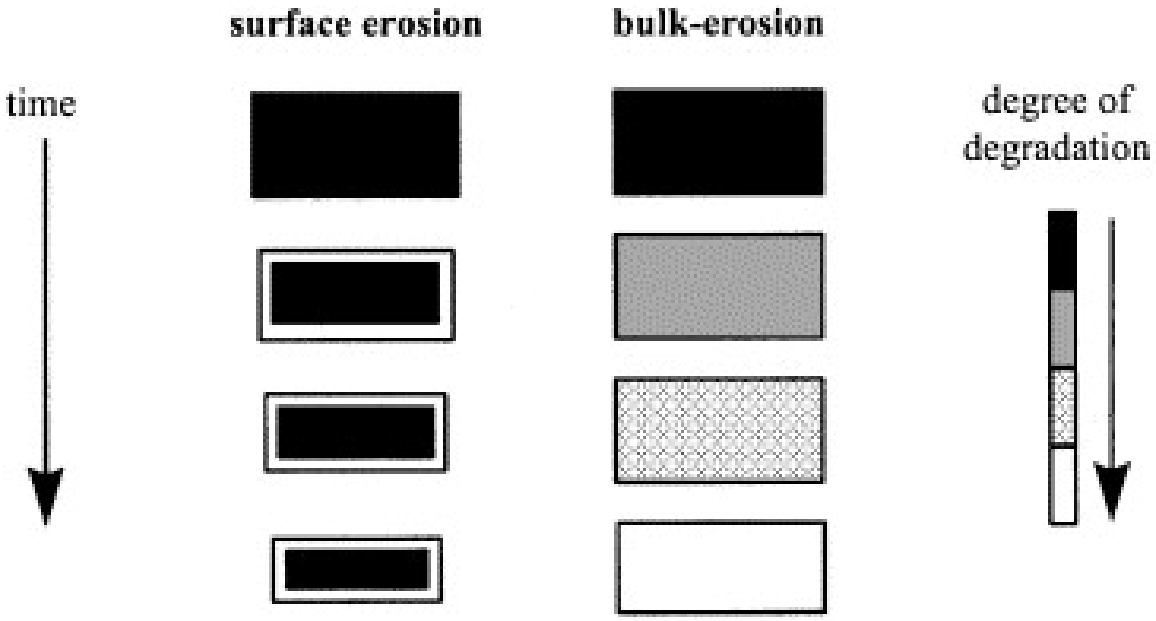


Figure 6: *Types of biomaterial erosion. Surface erosion maintains the properties of the bulk material while the outskirts of the structure are dissolved away. Bulk erosion leads to homogeneous dissolution behavior in which the structure loses its mechanical properties throughout.*[29]

As the polymers are degraded within the structure in bulk erosion, space is created for smaller chains to diffuse out and lead to loss of mass.[28] The presence of smaller chains throughout the structure leads to significant loss of mechanical properties at a quicker rate than mass loss. Surface eroding polymers exhibit linear erosion behavior as degraded chains diffuse instantly and the loss is reflected in mass.[29] Bulk eroding polymers exhibit a period of no mass loss, followed by an exponential decrease in mass as diffusion of small chains becomes dominant.[29]

### 1.5.3 Dissolution Modeling Methods

A common method implemented for modeling mass and molecular weight loss of a polymer is through Monte Carlo analysis. Monte Carlo analysis allows for simulation by assuming that the dissolution of individual chains occurs on a random basis with a probability defined by an exponential distribution. The use of an exponential distribution reflects the higher chance of a chain to dissolve as the time progresses due to easier accessibility to the chain over continuous erosion of neighboring molecules. The method, introduced by Gopferich et al., concentrates on a rectangular cross section of the bulk material and divides the cross section into individual pixels. The pixels represent components of the material that will degrade, with a higher number of pixels leading to more accurate results. Each pixel is given a total of three states: non degraded, degraded, and eroded.[30] Initially, all pixels are considered non degraded and the lifetime for each pixel is predefined. The following equations represent the process.[30]

The lifetime of an individual pixel is given by the exponential distribution

$$e(t) = \lambda \mathrm{e}^{-\lambda t} \tag{1}$$

The expected value of a given pixel degrading is therefore defined by

$$e(t)_{\text{expected}} = \frac{1}{\lambda} \tag{2}$$

assuming that the degradation of each pixel is a Poisson process, the expected value for $n$ pixels is given by

$$e(t)_{expected_n} = \frac{1}{\lambda} + \frac{1}{2\lambda} + \frac{1}{3\lambda} + \frac{1}{4\lambda} + ... + \frac{1}{n^2\lambda}. \tag{3}$$

Simplifying the summation further provides

$$e(t)_n = \lambda \ln(n^2) e^{-t\lambda \ln(n^2)}, \tag{4}$$

and solving for $t$ provides the time of degradation for an individual pixel depending on a randomly generated value, allowing for implementation of a Monte Carlo analysis:

$$t = \frac{1}{\lambda \ln(n^2)} \ln(1 - \epsilon) \tag{5}$$

where $e(t)$ is the expected probability of pixel degradation, $t$ is the time at which pixel degrades, $\lambda$ is the chemical rate constant, $n$ is the length of grid (pixels), $\epsilon$ is a randomly generated number. The follwing assumptions were made: 1) Degradation of individual pixels is a Poisson process. 2) Lifetime of each pixel is exponentially distributed.

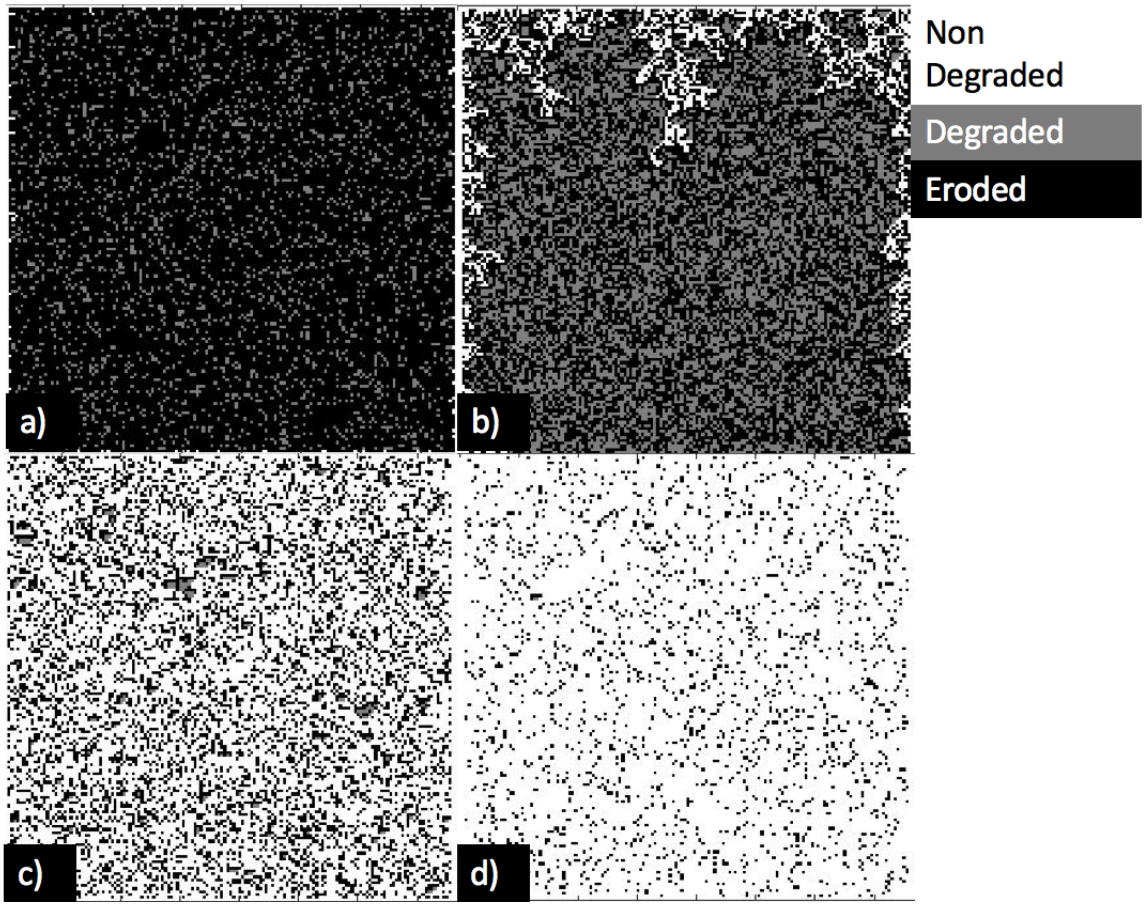


Figure 7: *Results of reproduced PLGA Monte Carlo dissolution modeling with a degradation constant of* $1.2*10^{-8}s^{-1}$ *(150x150 pixels) a) 1 week in phosphate buffered saline (PBS) with 99% mass and 86% molecular weight remaining. b) 4 weeks in PBS with 92% mass and 55% molecular weight remaining. c) 8 weeks in PBS with 32% mass and 30% molecular weight remaining. d) 16 weeks in PBS with 9% mass and 9% molecular weight remaining.*[30]

The Monte Carlo approach to degradation modeling is computationally inexpensive and accurate for simplified systems. Additionally, it solely depends on the rate constant of the chemical reaction, not considering the effect of cyclic loading, or varied geometry on the dissolution rate. The Monte Carlo analysis can be implemented to study the effect of porosity on the bioabsorbable cuff. Additional methods, such as the Boltzmann lattice method,[31] have been utilized for dissolution modeling but become computationally expensive when geometry and cyclic loading

is accounted for. For the purpose of studying the effects of pulsatile flow and the complex geometry on the degradation behavior of the cuff, a more complex algorithm will be required.

#### 1.5.4 Fabrication Techniques

The proper fabrication technique to create the transition of circular to elliptical cross section is important for the success of the bioabsorbable cuff. An effective technique will allow for changes in wall thickness, ellipse dimension, and cuff length. The technique should also allow for mixing of multiple polymers and the introduction of porosity to manipulate the dissolution rate of the cuff. Previous studies implemented simple geometry molds, 3D printing, and injection molding. Due to the easily achievable melting temperature of most biodegradable polymers, creating rectangular or circular molds becomes a simple process. The molds are filled with the melted biomaterial and left at room temperature to allow the biomaterial to solidify. The technique does not allow for creation of complex geometries such as the circular to elliptical transition shown in Fig.6.
Three-dimensional printing, and more specifically, selective laser sintering (SLS), has been implemented in creating more complex structures. In one such instance, polycaprolactone (PCL) micro-particles were extruded from a sintering station to create multi-dimensionally oriented porous structures. The structures were varied between rectangular blocks and cylinders.[32] The 3D printing approach expands the range of geometries and would allow for patterning of the bioabsorbable cuff if mechanical or dissolution properties will need to be modified further.

MIT applied an industrial injection molding machine to create complex geometries with PCL.[33] The process is illustrated below.[34]

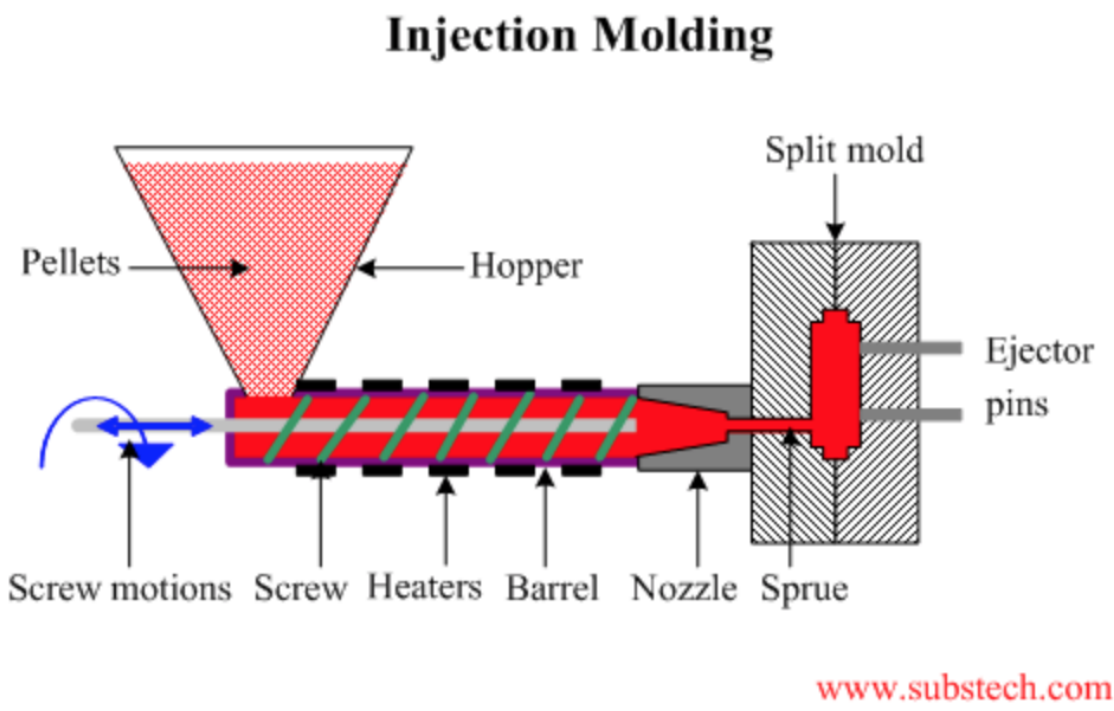


Figure 8: *Injection molding diagram. The PCL pellets are inserted in the reserve. As the pellets drop into the heated barrel and melts the screw motion pushes the melted material towards the constricted nozzle. The constriction of the nozzle with the applied force of the screws pressurizes the PCL and injects it into the split mold, overcoming the viscous nature of melted PCL.*[34]

The injection molding procedure is effective in creating large scale complex geometries but is limited in the creation of smaller features. The limitation arises due to the high viscosity of melted PCL which prevents the PCL from penetrating micron scale features and instead leads to back-flow.

### 1.6 Material Porosity

The introduction of porosity into polymer materials serves as a effective method of engineering mechanical and dissolution properties. The ability to control pore size and pore concentration creates a wider range of values to which the dissolution and mechanical properties can be optimized. To understand the

application of porosity to fabrication of a bioabsorbable cuff some porosity techniques as well as their effects on biomaterials properties must be understood.

### 1.6.1 Porosity Techniques

An overview of porosity techniques is important due to the effect that these techniques have on morphology, which in turn affects the biomaterial properties. The most common methods include particle leaching, gas foaming with $CO_2$ , electrospinning,and 3D printing.[35] The techniques cover pore diameters ranging between 15-500 µm.

Particle leaching, requiring by far the fewest resources and exhibiting limited flexibility, is initiated by exposing the biomaterial to a dissolving fluid. Common fluids include ethyl acetate, chloroform, acetone, and methanol. Once the material is dissolved, a water soluble powder is added to the solution at a concentration that leads to a specific porosity. The chosen powder must be of a specific particle diameter that is equivalent to the desired pore diameter. In gas foaming with $CO_2$ a sample is pressurized in a $CO_2$ pressure vessel.[36] The pressure is set so the $CO_2$ is in the supercritical region. Prolonged exposure at high pressure allows $CO_2$ to dissolve into the solid biomaterial. Once material absorbs enough $CO_2$ , its glass transition temperature ($T_g$) is lowered making a polymer/gas solution.[36] Pressure is rapidly decreased and as $CO_2$ becomes less soluble, bubble nucleation proceeds. As bubbles become larger and diffuse, $T_g$ increases until it equilibrates with the temperature of the chamber and bubbling ends.[36] The application of $CO_2$ foaming allowed for creation of particles between 30 µm-100 µm and porosities up to 93% depending on the temperature of the vacuum chamber, degassing rate, and saturation pressure.[36]

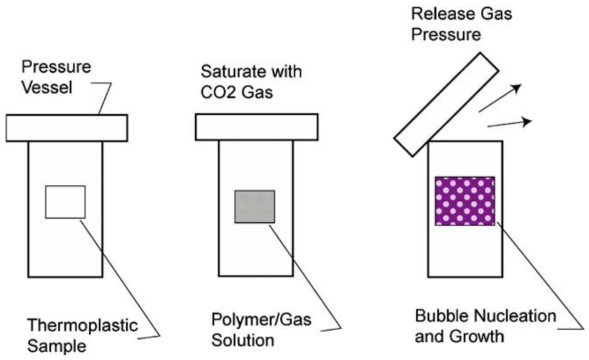


Figure 9: *The three main steps of the gas foaming method.*[36] *The polymer material is placed in the pressure vessel (left), after which the vessel is filled with* $CO_2$ *and pressurized (middle). As the pressure is rapidly dropped, bubble nucleation forms pores within the material (right).*[36,37]

In the last decade, electrospinning has gained popularity in tissue engineering applications. In this process, a high voltage source is used to polarize the extruded material with an opposing charge to the surface on which the material is being extruded, causing the acceleration of the material onto the surface. The resulting fibers can vary in diameter between micrometers down tens of nanometers.[38] By controlling the spacing between fibers, pores can be created. Even though electro-spinning mimics the native biological environment of the extracellular matrix,[38] the inability to control exact pore size and to create pores of specific geometries makes it less desirable for fabrication of the bioabsorbable cuff. Additionally, the creation of thin sheets of porous biomaterial is resource intensive and expensive. The 3D printing of biomaterials is another method gaining popularity and has been applied to create porous structures by combining particle leaching and simple manipulation of printing geometry to create a porous scaffold (as previously mentioned). In the study of Tan, et al. PCL and PVA particles of specific diameters were mixed and printed in different ratios.[39] Upon print completion, the PVA was dissolved in water to create the porous structures. The

pores were of random size and shape ranging between 100-500 µm, depending on the mixing morphology of PVA and PCL.[39] The 3D printing techniques are definitely viable options for creation of the bioabsorbable cuff upon better control of pore size, as they are relatively inexpensive and will allow for creation of complex geometries.

### 1.6.2 Properties of Porous Materials

As expected, introducing porosity leads to changes in the material's mechanical and dissolution properties. Additionally, methods used for creation of such porous structures affect the properties. The introduction of porosity through salt leaching techniques into PCL was found to reduce the elastic modulus from 1.85 MPa to 0.24 MPa when porosity was changed from 46% to 85%.[40] Porosity introduction using the 3D printing method with PVA and PCL led to a storage modulus change from 0.19 MPa to 0.03 MPa when porosity was changed from 50% to 60%.[39] The 3D printing of porous structures by printing 1D, 2D, and 3D orthogonally oriented architecture creates a range of properties in the figure below.

Mechanical property assessment of bulk and porous SLS processed PCL.

| | Property | Unit | SLS | | | | | Injection molding[2] |
|---|---|---|---|---|---|---|---|---|
| | | | Solid gage section | | Porous gage section[1] | | | |
| | | | // | ⊥ | 1D | 2D | 3D | |
| Tension | Elastic modulus, $e$ | MPa | 363.4 ± 71.6 | 343.9 ± 33.2 | 140.5 ± 19.6 | 42.0 ± 6.9 | 35.5 ± 5.8 | 430 |
| | 0.2% Offset yield strength, $\sigma_Y$ | MPa | 8.2 ± 1.0 | 10.1 ± 1.5 | 3.2 ± 0.6 | 0.67 ± 0.08 | 0.67 ± 0.06 | 17.5 |
| | Strain at yield, $\varepsilon_Y$ | – | 0.024 ± 0.006 | 0.031 ± 0.002 | 0.024 ± 0.001 | 0.017 ± 0.002 | 0.020 ± 0.002 | – |
| | Ultimate tensile strength, $\sigma_{UT}$ | MPa | 10.5 ± 0.3 | 16.1 ± 0.3 | 4.5 ± 0.4 | 1.2 ± 0.2 | 1.1 ± 0.1 | – |
| | Strain at break, $\varepsilon_B$ | – | 0.043 ± 0.007 | 8.0 ± 0.3 | 0.095 ± 0.022 | 0.092 ± 0.022 | 0.096 ± 0.025 | > 7 |
| Compression | Elastic modulus, $E$ | MPa | 297.8 ± 7.1 | 317.1 ± 3.9 | 133.4 ± 2.6 | 12.1 ± 0.5 | 14.9 ± 0.6 | – |
| | 0.2% Offset yield strength, $\sigma_Y$ | MPa | 12.5 ± 0.3 | 10.3 ± 0.2 | 4.25 ± 0.05 | 0.45 ± 0.01 | 0.42 ± 0.03 | – |
| | Strain at yield, $\varepsilon_Y$ | – | 0.052 ± 0.003 | 0.037 ± 0.002 | 0.0370 ± 0.000 | 0.0376 ± 0.001 | 0.0268 ± 0.003 | – |
| | Ultimate compressive strength | MPa | 38.7 ± 0.3 | 38.80 ± 0.66 | 10.0 ± 0.62 | 0.60 ± 0.00 | 0.60 ± 0.00 | |

*Note:* $\mu \pm \sigma$ where $\mu$ denotes the mean and $\sigma$ denotes the standard deviation ($n = 6$).
[1] Porous compressive specimens tested parallel to SLS build direction, porous tensile specimens tested perpendicular to SLS build direction.
[2] Reported by Perstorp Caprolactone, tests were conducted at a strain rate of 10 mm min$^{-1}$ to determine $E$ and 100 mm min$^{-1}$ in all other cases.

Figure 10: *Porous and bulk PCL tensile and compressive properties. The porosities for the tensile specimens were 56.87%, 67.4% and 83.3% 1D to 3D, while the porosities for the compressive specimens were 51.1%, 68.5% and 80.90%, 1D to 3D.*[32]

## 1.7 Research Aims

**Aim 1. Development of a Fabrication Method**. The initial goal is to utilize silicone rubber to create prototypes of cuff geometry illustrated in Fig. 4 in which circular outer cross-sections converge to a cylindrical cross-section in the center. The following goal is to utilize PCL to create the same cuff geometry with a method that will allow for introduction of porosity. The rationale is to create silicone prototypes that can be implemented in animal studies as well as optimize the fabrication method with polycaprolactone to allow for creation of complex geometry and control of dissolution parameters.

**Aim 2. Characterizing Effects of Cyclic Loading on Material Dissolution**. The dissolution properties of polycaprolactone and the effects of different environments on the these properties will be studied. Porous polycaprolactone scaffolds will be tested under cyclic loading to mimic the pulsatile pressure of the heart and observe the effects on dissolution rate. The rationale is to obtain data that will allow for controlled dissolution of the cuff as well as relate porosity to the mechanical response of the cuff to cyclic loading.

**Aim 3. Simulate Flow Through Porous Material**. Computational software (ANSYS) will be utilized to simulate the diffusion of blood through sections of porous material. The effect of pore diameter, porosity, and section thickness on flow rate through the porous material due to dynamic blood pressure will be modeled. The rationale is to develop an understanding of the effect of cuff thickness and porosity on cuff dissolution. Further, such information will be used as a guide for optimizing the mechanical and dissolution properties of the cuff.

# 2 Methods

## 2.1 Fabrication Methods

The fabrication method is of importance for the design of the cuff because it will determine the degree to which the dissolution and mechanical properties of the cuff can be engineered. In the following sections, the prototyping stage with silicone rubbers, failed fabrication techniques with PCL, and the chosen fabrication method that allows for porosity manipulation and creating of complex geometry with PCL will be presented.

### 2.1.1 Fabrication with Silicone Rubbers

The prototypes developed from silicone rubbers will be implemented in ex-vivo experiments as well as animal trials for analysis of the flow through the shunt. Since silicone rubbers are meant for fabrication, they are a convenient starting platform for developing the final fabrication technique. The applied silicone rubbers were Oomoo 30 and Eco-flex 30, (Smooth-On Inc.); Oomoo exhibits a pot life of 30 minutes and cure time of 6 hours, with a Shore hardness of 30A, lavender color, 250% elongation at break, and viscosity of 4250 mPa s.[41] Eco-flex exhibits a pot life of 45 minutes and cure time of 4 hours, with a Shore hardness of 30A, translucent, 900% elongation at break, and viscosity of 3000 mPa s.[41] Castaldo Plast-O-Wax Injection Wax (Rio Grande) melts between 68 °C-71 °C and is solid at room temperature.[42]

Due to the existence of an elliptical center with a larger radius on the y-axis than the radius of the circular ends of the cuff, a difficulty arises in pulling out the inner mold one the silicone cures. To overcome the issue the fabrication procedure implements wax melting. The wax maintains the elliptical geometry while at room temperature, allowing the cuff material to cure, after which the wax is melted away

to create the void. The desired cross section of the cuff is illustrated below.

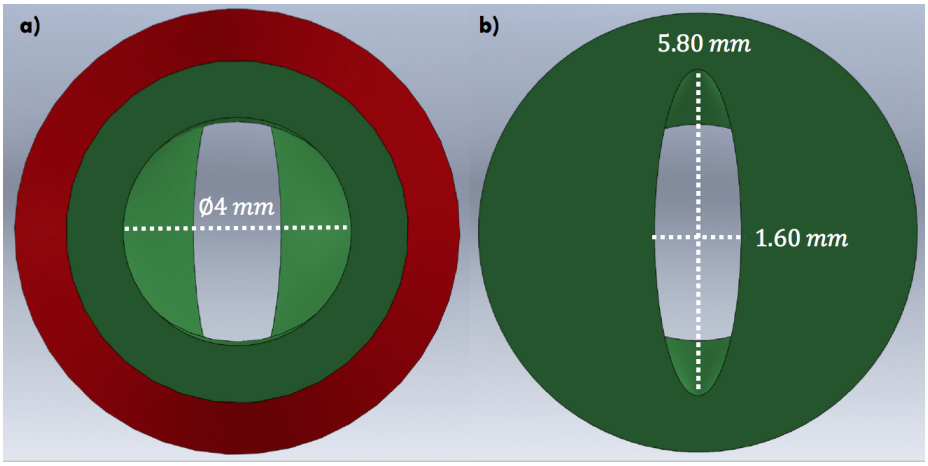


Figure 11: *The outside and center cross sections of the cuff. a) The circular cross-section of* 4 mm *in diameter at the ends of the cuff, equivalent to the diameter of the Gore-Tex shunt. b) The internal elliptical cross-section that reduces the area while maintaining the circumference with an x-axis diameter of* 1.6 mm *and y-axis diameter of* 5.8 mm.

The following components were used in fabrication:

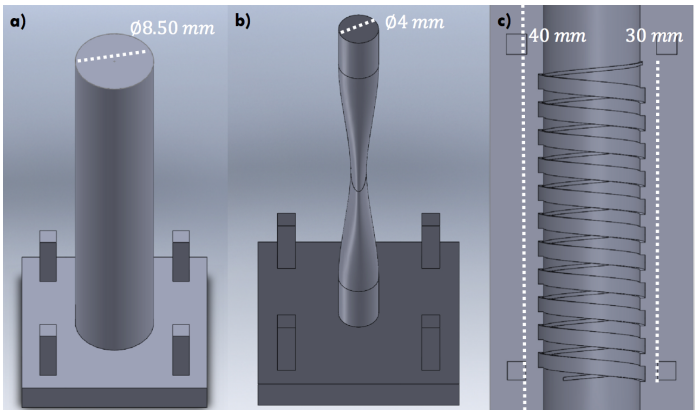


Figure 12: *The three components required for cuff fabrication with silicone. a) Sacrificial cylindrical mold* 40 mm *in height and* 8.50 mm *in diameter. b) Sacrificial elliptical mold with a* 30 mm *convergence towards the elliptical center and a diameter of* 4 mm. *c) Outer mold* 40 mm *in height with a* 30 mm *section that can be manipulated with different designs. All the molds are* 10 mm *longer than the true cuff to allow for extra space on the ends, preserving the homogeneity of the true cuff.*

A specific order is followed to allow for casting a single layer of material or co-casting. The ability to co-cast allows for fabrication out of multiple materials with different properties. Multiple properties can be used to create a stronger outer layer with a more flexible inner layer to allow for pulsatile expansion. Additionally, the versatile method could be optimized for fabrication with multiple biodegradable materials with different mechanical and dissolution properties, further expanding the capability to engineer the cuff. The fabrication process is outlined below.

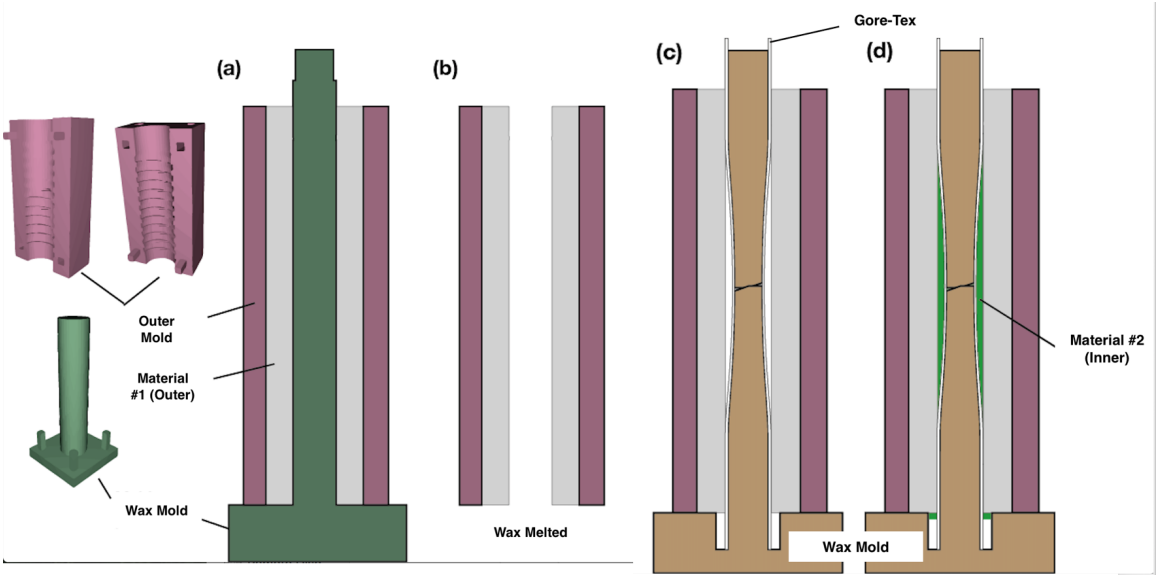


Figure 13: *Four steps of rubber fabrication. a) The straight cylindrical mold is inserted between the two outer molds and material is casted into the space in between using a vacuum chamber. b) Upon curing of surrounding silicone rubber the structure is exposed to* 75 °C *to melt the sacrificial cylindrical mold. c) The Gore-Tex shunt is pulled over the elliptical wax mold and both are inserted into the outer mold with the initial material on the side walls. d) The second material is casted into the remaining space using a vacuum chamber, after which the wax mold is melted away.*

For single material fabrication, the process can begin at step c) in which the full thickness of the remaining silicone structure is made up of the same material. The structures fabrication with this method utilizes Oomoo as the outer layer, due to its higher stiffness and darker color. Eco-flex was utilized in the inner later due

to higher flexibility allowing for expansion of the Gore-Tex during pulsation.

### 2.1.2 Injection Molding of PCL

Using PCL for fabrication is significantly more challenging than silicone. The high viscosity of melted PCL makes it incompatible with traditional vacuum pumping methods. The smaller geometry of the cuff complicates the technique due to higher resistance to the viscous flow of melted PCL in the smaller features. Polycaprolactone of 80 000 Da was purchased from Plastimake. An attempt to overcome the viscous forces of Polycaprolactone, 80 000 Da (Plastimake), was made with implementation of injection molding. Using this technique, the PCL was melted and injected into an aluminum mold with a silicone mold creating the internal elliptical geometry. The setup is illustrated below.

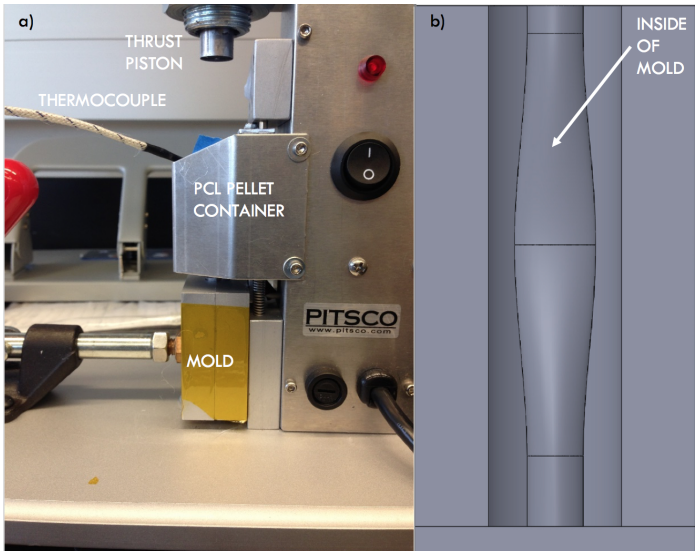


Figure 14: *Set up for injection molding of PCL. a) The pressure applicator is pushed into the PCL pellet container which contains melted PCL. The thermocouple is used to maintain the temperature below* 100 °C *and prevent PCL burning. The melted PCL enters the mold under pressure. b) CAD model of the inside of the mold. The elliptical constriction is shown, with PCL filling up the void around the inner elliptical piece.*

### 2.1.3 PCL "Jelly Roll" Technique

The "jelly roll" technique involves wrapping the biodegradable material around a cylindrical structure, forming layers of material resembling a jelly roll structure. In this specific application, PCL was pressed into thin sheets between 500-125 µm by exposing it to temperatures of 100 °C under compressive forces. The process is illustrated below.

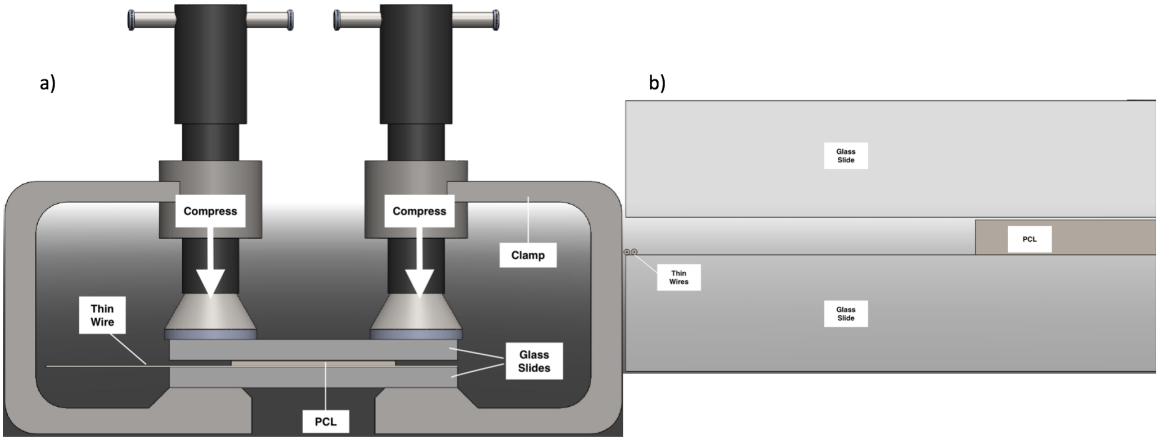


Figure 15: *Simple representation of the jelly roll technique. a) Two glass slides are pressed together with a pair of clamps on both sides. PCL and thin wires are placed in between the slides, with the thin wires determining the thickness of resultant PCL sheet. b) A close up of the PCL and glass interface. As the glass slides are pressed together against the melted PCL, the PCL is compacted into a thin sheet until the glass presses against the thin wires and limits further thinning of PCL.*

The wires used were 500 µm, 250 µm, and 125 µm in diameter, resulting in the range of sheet dimensions mentioned earlier. Due to the flexibility of the resulting sheets they can be wrapped around desired geometry. The sheets were first exposed to 50 °C water and then wrapped. The exposure to higher temperatures further reduces the rigidity of the sheets and allows them to conform to the geometry of the elliptical mold in Fig.14. To fuse the resulting layers together, the structure is submerged in 60 °C water, melting the interface between the layers and creating a single continuous layer.

## 2.2 Porosity Introduction

Salt leaching was the chosen porosity introduction technique used for the proof-of-concept cuff studies. Even though other techniques allow for more control of particle size and porosity in complex geometry, the simplicity of salt leaching is satisfactory for fabrication of PCL blocks to test the effect of cyclic loading on dissolution properties. Other porosity introduction methods will be described at the point of porous cuff fabrication.

A sample of Morton ExtraFine 200 Salt (Morton Salt Inc.) with more than 92% of NaCl particles passing the 75 µm mesh standard. Standard ethyl acetate solution (Spectrum Laboratory Products Inc.) is used as the solvent for PCL while allowing the salt particles to remain insoluble and occupy their respective volumes once the ethyl acetate is dissolved.

### 2.2.1 Technique

The porous PCL was prepared using a traditional technique in which PCL particles were dissolved in ethyl acetate to a concentration of 10% (weight/volume).[43] The NaCl particles were then incorporated in different concentrations corresponding to different porosities.[43] The mass ratio of PCL to NaCl did not follow the theoretical calculations for void volume due to the settling of NaCl particles during the evaporation of ethyl acetate, concentrating the NaCl particles to a smaller region of higher porosity. All mixtures were prepared in 50 mL of ethyl acetate and 5 g of PCL. Addition of 20 g, 28 g, and 45 g of NaCl, led to porosity of 70%, 80%, and 90%, respectively.

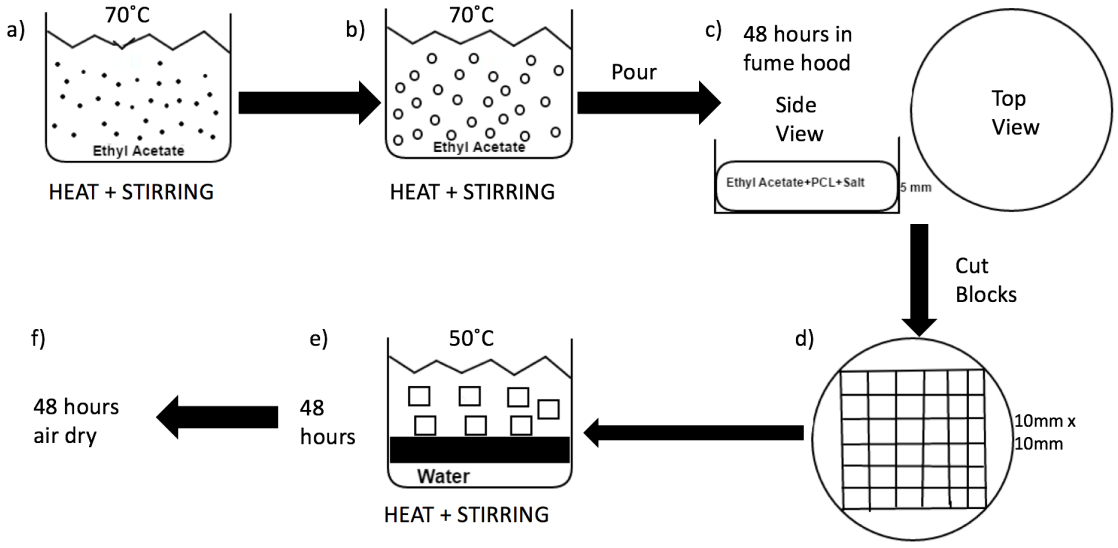


Figure 16: *Porosity introduction procedure. a) NaCl is inserted into an ethyl acetate solution and stirred with a magnetic stirrer at* 70 °C. *The mass of NaCl inserted depends on the desired porosity, as outlined in the previous paragraph. b)* 5 g *of PCL is inserted into the mixture after the salt has homogeneously distributed. The heating and stirring is continued until the PCL is completely dissolved in solution. c) The solution is removed from the heat and stirring and poured into a circular glass plate to a* 5 mm *height. The ethyl acetate is allowed 48 hours to evaporate. d) The remaining solid disk is sliced into* 10 mm x 10 mm *blocks with a razor blade. e) The blocks are submerged into* 50 °C *water with stirring to dissolve the salt. The water was regularly changed every 8 hours. f) After completion of leaching, the PCL blocks are allowed to air dry at room temperature outside of the fume hood.*

The chosen height of the PCL blocks is important in maintaining homogeneous porosity throughout the block. During fabrication of higher thickness blocks a formation of a non-porous layer at the top of disk was observed due to settling of salt before ethyl acetate evaporation. Glass was utilized in all applications because ethyl acetate is highly reactive with common plastics.

### 2.2.2 Validation

The porosity of the resulting blocks was tested using Archimede's principle. The mass of the dry solid is recorded ($M_{PCL}$). The solid is placed in ethanol under vacuum to force the ethanol to enter the pores. Ethanol is used due to its low surface tension which allows it to easily enter the smaller pores. The scaffold is removed from ethanol and the edges are gently wiped to remove excess ethanol on the surface. The scaffold is once again weighed after degassing in the vacuum ($M_{PCL+Ethanol}$). The following equations were used to calculate porosity.

$$V_{PCL} = \frac{M_{PCL}}{\rho_{PCL}}, \tag{6}$$

$$V_{Ethanol} = \frac{M_{PCL+ethanol} - M_{PCL}}{\rho_{ethanol}}, \tag{7}$$

and

$$\epsilon = \frac{V_{ethanol}}{V_{ethanol} + V_{PCL}} \tag{8}$$

where

$V_{PCL}$: Volume of PCL

$V_{ethanol}$: Volume of Ethanol

$M_{PCL}$: Mass of PCL

$M_{PCL+Ethanol}$: Mass of PCL and Ethanol

$\rho_{PCL}$: Density of PCL: $1.145\,\mathrm{g\,cm^{-3}}$

$\rho_{ethanol}$: Density of Ethanol: $0.789\,\mathrm{g\,cm^{-3}}$

$\epsilon$: Void volume (porosity)

## 2.3 Cyclic Loading

Even though dissolution times for biomaterials *in vivo* have already been studied, there is a lack of information on dissolution under cyclic loading. As the

cuff will be placed around a shunt that is exposed to fluctuations between diastolic and systolic pressure, the effects of cyclic loading on dissolution rate must be accounted for. The porous PCL blocks created in the previous section will be implemented in an experimental set up meant to mimic the pressure fluctuations experienced in the body.

### 2.3.1 Analysis

Due to the range of congenital heart defects, the pressures exerted on the cuff range. Therefore, well known adult vital signs of a heart rate of 60 bpm, systolic pressure of 120 mmHg, and diastolic pressure of 80 mmHg were chosen as the physiological values that will be replicated ex-vivo and simplify the experimental design. In future experiments the parameters can be changed to 100 bpm, systolic pressure of 90 mmHg, and diastolic pressure of 65 mmHg, to exactly mimic the heart rate and pressure of an infant[44] and further changes can be made to mimic vital signs of each defect. The pressure acting on the cuff can be approximated by assuming that the cuff is a cylindrical tube with blood flow applying radial pressure from within. The radial pressure is translated to radial, circumferential (hoop), and axial stress. In the case of a cylinder with open ends the axial stress can be neglected. The thin wall assumption, often used to simplify the pressure-stress relations in cylindrical structures, cannot be used here because the wall thickness is well over 5% the cuff's diameter, the traditional threshold of applying this assumption. Assuming the wall thickness is always greater than 500 µm , the stresses will have to be calculated for a thick-walled tube using *Lameé's equations*.

$$\sigma_h = \frac{p_i r_i^2 - p_o r_o^2}{r_o^2 - r_i^2} + \frac{(p_i - p_o) r_o^2 r_i^2}{(r_o^2 - r_i^2) r^2} \tag{9}$$

$$\sigma_r = \frac{p_i r_i^2 - p_o r_o^2}{r_o^2 - r_i^2} - \frac{(p_i - p_o) r_o^2 r_i^2}{(r_o^2 - r_i^2) r^2} \tag{10}$$

$\sigma_h$: Hoop stress

$\sigma_r$: Radial stress

$p_i$: Pressure inside tube

$p_o$: Pressure outside tube

$r_i$: Inner radius

$r_o$: Outer radius

Assuming a thickness of 500 µm, ambient external pressure, an inner radius of 2 mm and evaluating the stresses on the inner circumference, the systolic and diastolic *hoop stresses* are 73 kPa and 48 kPa above ambient, respectively. The systolic and diastolic radial stresses of 16 kPa and 10.67 kPa, respectively, remain close to the radial pressure of 120 mmHg and 80 mmHg applied. In our experimental setup to test the dissolution of porous PCL, we employ the hoop stress to load porous PCL samples and represent the largest stresses applied on the cuff by the cardiac cycle. Application of this cardiac cycle driven hoop stress onto square cross-sectioned PCL blocks each with a cross-sectional area of 100 $\text{mm}^2$, for example, leads to the following forces: $F(t) = A\sigma(t)$ where $F(t)$ is the compressive force applied to each PCL block of cross-sectional area $A$ to match the tensile hoop stress seen in the cuff, $\sigma_{\text{diastolic}} = 48\,\text{kPa}$ producing $F_{\text{diastolic}} = 4.86\,\text{N}$, and $\sigma_{\text{systolic}} = 73\,\text{kPa}$ producing $F_{\text{systolic}} = 7.30\,\text{N}$.

### 2.3.2 Experimental Model for Cardiac Cycle Loading of Porous Cuff Material

The application of cyclic stresses to porous PCL samples was accomplished by combining the static force due to gravity for the diastolic based hoop stress and a harmonic magnetic force to generate the additional load necessary for systolic hoop stress as shown in Fig.17. As shown in Fig.17, an iron mass weighing 500 g was placed on top of a single PCL block to apply the needed 4.86 N. As the electromagnet voltage is oscillated at 1 Hz, equivalent to 60 bpm, the force applied

on the PCL block oscillates between 4.86 N and 7.30 N. The setup is illustrated below.

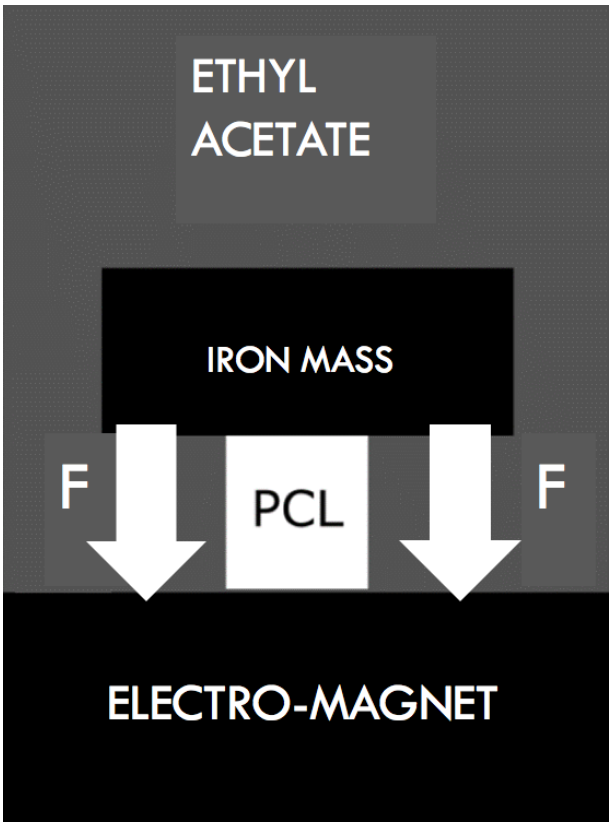


Figure 17: *Cyclic loading set up. The PCL is surrounded by ethyl acetate as its dissolving fluid. Ethyl acetate, and excellent solvent for PCL, was used to reduce the time needed to conduct the experiments. As the power to the electro-magnet oscillates at* 1 Hz *the force applied on the PCL fluctuates between the diastolic and systolic equivalent.*

The iron mass was placed atop the PCL blocks, with the force sensor between the iron mass and the PCL. The distance between the iron mass and the magnet, as well as the power applied to the electro-magnet, determine the force applied on the PCL. A 12 V cylindrical DC-powered electro-magnet with a maximum pull of 800 N was obtained from McMaster-Carr (part # 5698K116) was used with a force sensor (Flexiforce A101, Tekscan) to verify the increased force applied on the PCL through the attraction of the iron mass. The voltage to the electromagnet was then adjusted

to 7.8 V to obtain a force of 7.30 N. The force sensor was connected to a computer via Arduino Due (Arduino). The force verification setup is shown in Fig.18 and the calibrated output force from the Arduino-based force sensor is provided in Fig.19.

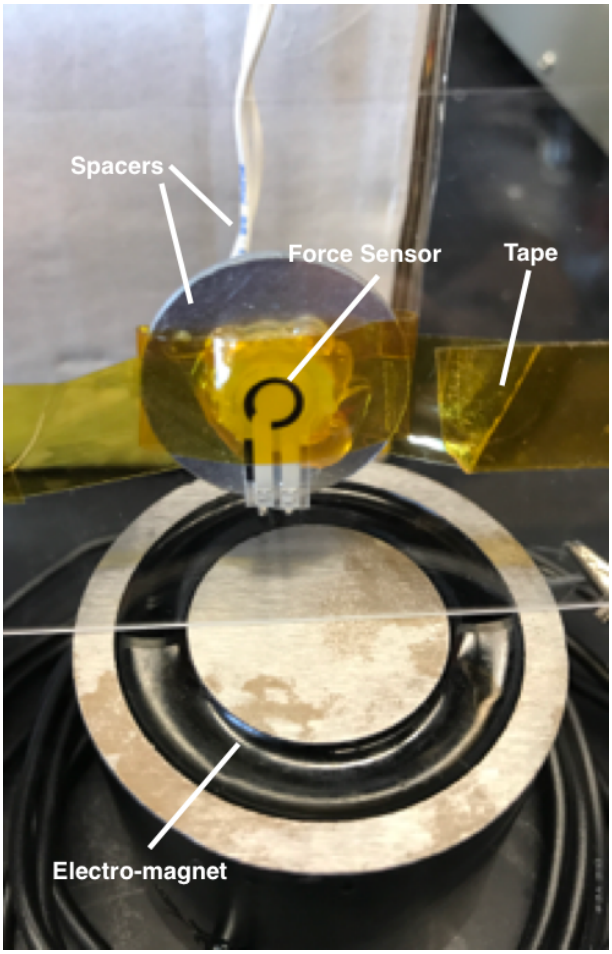


Figure 18: *Force verification set-up. The electromagnet is powered by a* 12 V *power supply. The force sensor is placed below a washer and glass slide that are used as spacers. The spacers are meant to place the iron mass* 5 mm *away. The washer also serves to balance the mass and distribute its weight on the force sensor.*

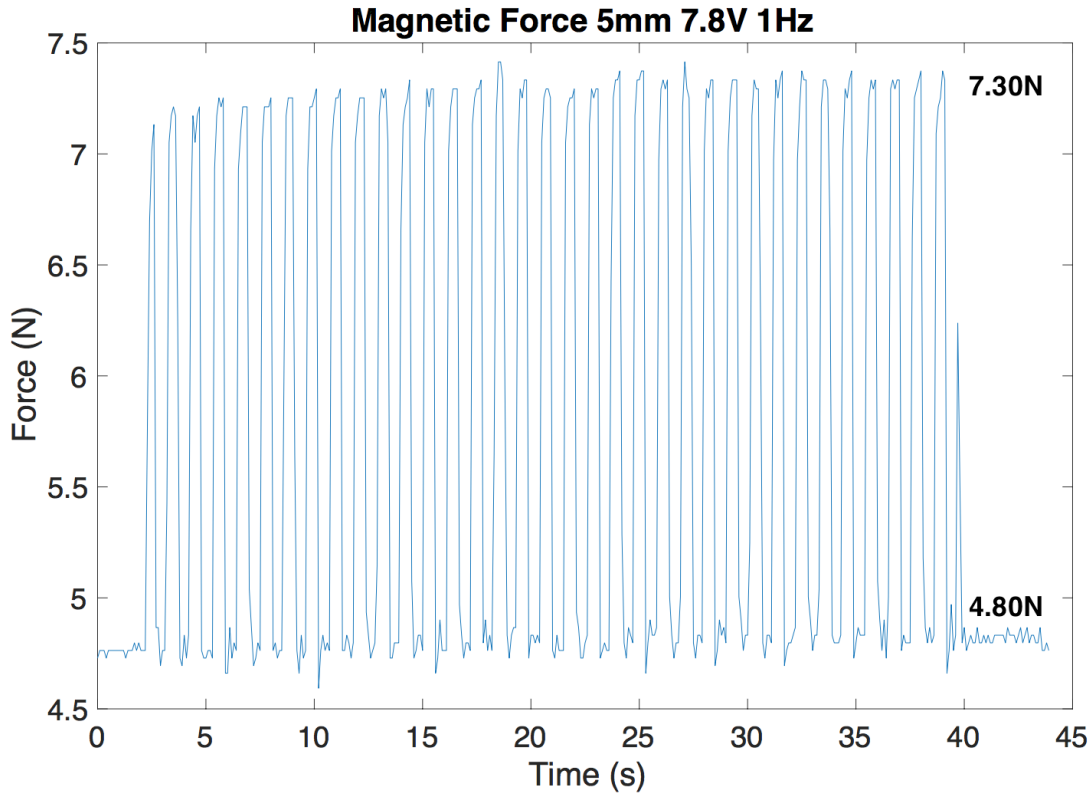


Figure 19: *The square wave generator drives the magnetic field at a frequency of* 1 Hz *between a systolic force of* 7.30 N *and a diastolic force of* 4.80 N *caused by the mass alone. A distance of* 5 mm *and a driving electromagnet voltage of* 7.8 V *will be maintained in the experimental setup with PCL.*

### 2.3.3 Square Wave Generator

The oscillating magnetic force was generated by using a square wave with an input voltage with a 50% duty cycle and a frequency of 1 Hz, producing the force variation shown in Fig.19. The simple custom circuit required to generate this signal is shown in Fig.20.

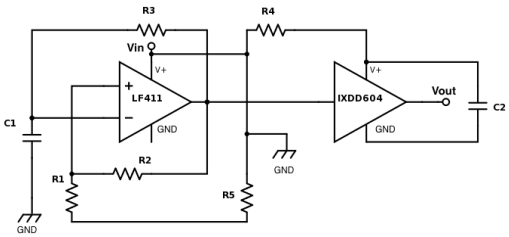


Figure 20: *Square wave generator schematic. The combination of LF411 and IXDD604 amplifiers creates a stable 50% duty cycle square wave oscillating between* 0 V *and the desired input voltage up to a maximum of* 12 V*. The combination of resistors and capacitors determines the generated frequency. A DC power source provides* $V_{in}$*, while* $V_{out}$ *is connected to the magnet and all components are connected to a common ground on the DC power supply.*

The following equations were used to determine the appropriate combination of resistors and capacitors for the desired frequency:

$$T = 2R_3C_1 \ln(\frac{1+\lambda}{1-\lambda}), \tag{11}$$

$$\lambda = \frac{R_1}{R_1 + R_2}, \tag{12}$$

and

$$F = \frac{1}{T}, \tag{13}$$

where $T$ is the period of the wave, $F$ is the frequency. The appropriate values for the system were $R_1$=8 kΩ, $R_2$=10 kΩ, $R_3$=50 kΩ for resistances, and $C_1$=10 µF for the capacitance. To ensure stability of the circuit and prevent negative voltage, a pair of additional resistors of $R_4$=0.68 kΩ, $R_5$=0.68 kΩ, and capacitor of $C_2$=0.001 µF were introduced.

An input of 7.8 V from a DC power source was connected to $V_{\text{in}}$ and the output square wave signal of the same amplitude, $V_{\text{out}}$, produced by the circuit was connected to the electro-magnet.

### 2.3.4 Cyclic Loading Experimental Procedure

The PCL blocks were initially placed in a beaker with ethyl acetate inside a vacuum chamber to draw the ethyl acetate into the pores. The dissolution of blocks was quantified by weighing the blocks every 15 min without loading and every 10 min under cyclic loading. The PCL blocks without loading were tested for 135 min while blocks under cyclic loading were tested until the block could no longer be properly weighed due to low mass. A standard laboratory scale (APX-200 Denver Instruments ±0.1 mg) was used for weighing the PCL blocks. The starting mass of PCL blocks ranged between 0.4 g and 0.8 g. Porosities of 70%, 80%, and 90% were used under no loading and cyclic loading conditions with $n = 5$ for each case. The experiments were carried out at 35 °C for dissolution times that are easier to measure.

## 2.4 Porous Flow Modeling Set Up

To understand the effect of PCL thickness, porosity, and pore diameter on dissolution, the flow of blood through porous PCL must be understood. As the flow rate through the material when used in the cuff increases, the material degradation and diffusion rates increase as well. The finite element method (ANSYS 17.2) was used to directly model this phenomenon by modeling the blocks as immersed in the blood and caused to flow through the pores from a dynamic pressure difference from one side of the PCL sample to the other. Blocks of different lengths, porosities, and pore diameters were used to determine their effect. The dynamic effect of the cardiac cycle on the shunt cuff manifests itself as a periodic squeezing and release of the PCL porous media, much like the periodic squeezing of a sponge: fluid is caused to flow in and out via this squeezing action, likely increasing the dissolution rate. To determine the upper bound for such an induced flow, a constant pressure difference across the block of 40 mmHg was applied in ANSYS to represent the

pulsation effect of blood pressure as illustrated in Fig.21.

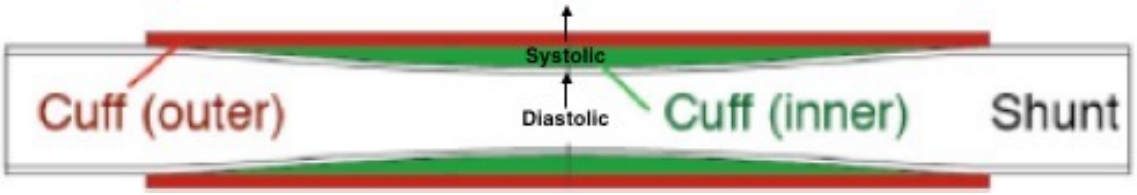


Figure 21: *Dynamic pressure illustration. The extra-vascular fluid passes into the cuff through passages purposely introduced in the far ends of the cuff and is partially pushed under systolic pressure. Therefore, the pressure driving the fluid through the pores can be modeled as a static* 40 mm*Hg.*

ANSYS combines the general fluid flow equations[45] that are used for all types of flow with a source term to define the effects of porous flow.[46] The source term is based on a viscous loss and a inertial loss term. Inertial losses through porous media arise due to the effects of turbulent flow, such as recirculation within the pore.[46] In the case of of the cuff the flow is assumed to be laminar due to the small pressure change driving the flow and a Reynolds number below 1. The assumption of laminar flow simplifies the source term to the empirical Darcy porous media flow model,[46]

$$u = \frac{Q}{A} = -\lambda \frac{\Delta P}{L} = -\frac{k \Delta P}{\mu L} \tag{14}$$

where $u$ is the flow velocity, $Q$ is the flow rate, $A$ is the flow area of porous media, $\Delta P$ is the pressure gradient across porous media, $\lambda$ is the mobility of porous media, $L$ is the length of porous media, $k$ is the permeability of media, and $\mu$ is viscosity.

To relate the effects of porosity and pore diameter to the flow model, the permeability term, $k$, needs to be defined in those terms. To do so, the capillary tube model for porous flow is applied, in which the capillary tubes represent the interconnected pore network with the assumption of constant radius and tube length longer than the length of the block.[47] In this model the porosity is defined by

the amount of capillary tubes per unit area, and the radius of the capillary tube defines the pore radius.[47] Assuming a random distribution of spherical pores throughout the system, the following expression for porosity is derived.[48]

$$\phi = \frac{n\pi R^2}{A} \tag{15}$$

where $n$ is the number of tubes per unit area and $R$ is the pore radius.

The flow rate through a capillary tube can be represented by the modified Hagen-Poiseuille equation as follows[48]

$$Q = \frac{\pi R^4 \Delta P}{8\mu\tau L} \tag{16}$$

where $\tau$ is tortuosity of the capillary tube defined by

$$\tau = (\frac{L'}{L})^2, \tag{17}$$

for which $L'$ is the length of capillary tube and $L$ is the length of system.

From empirical data the tortuosity can be approximated by a value of $\frac{25}{12}$.[48] Equating Darcy flow through porous media to the modified Hagen-Poiseuille model and applying the definition of porosity given in eqn.(15), the following expression for $k$, permeability, is obtained:[48]

$$k = \frac{3\phi R^2}{50}. \tag{18}$$

The permeability value was calculated for a range of porosities and pore diameters and imported into ANSYS. The properties of the fluid used in the model need to also be specified. Blood was used as the fluid body and was simulated as a non-Newtonian shear thinning fluid. where there is a decrease in viscosity as the shear rate increases. As the change in fluid velocity with respect to distance from the wall boundary increases, the blood becomes less viscous. The four most

common models for blood simulation are the power-law model, Casson model, Cross model, and Carreau-Yasuda model.[49] The power-law model is valid if the shear rates are in the region where the viscosity of the fluid truly varies as the power of shear rate. Using the power-law $\mu \to 0$ as $\dot{\gamma} \to \infty$, in which $\dot{\gamma}$ is the shear rate, underestimates the viscosity at high shear rates. As $\dot{\gamma} \to 0$ the viscosity $\mu \to \infty$, overestimating the viscosity of the fluid at low shear rates.[49] The Casson model follows blood behavior closely for $\dot{\gamma} > 1\,\mathrm{s}^{-1}$ but $\mu \to \infty$ as $\dot{\gamma} \to 0$[49,50]

Both the Cross and the Carreau-Yasuda model avoid the issue of divergence to $\infty$ or convergence to 0 across the complete range of $\dot{\gamma}$ by using four approximating parameters. Both models account for the Newtonian regions of blood and the power relationship between the viscosity and shear rate, well correlated to experimental data. Due to the availability of values for the 4 parameters needed for the Carreau-Yasuda model, it was chosen as the input model for ANSYS. The expression for viscosity as a function of shear rate in the Carreau-Yasuda model[50] is given by

$$\mu(\dot{\gamma}) = \mu_\infty + (\mu_0 - \mu_\infty)(1 + (\lambda\dot{\gamma})^a)^{\frac{n-1}{a}} \tag{19}$$

where $\mu_0$ is the viscosity at low shear rates, $\mu_\infty$is the viscosity at high shear rates, $\lambda$ is an empirically determined time constant, $a$ is an empirically determined constant, and $n$ is an empirically determined constant.

The empirically determined time constants define the behavior for the fluid between the asymptotic regions of $\mu_\infty$ and $\mu_0$.[50] The following values were chosen for the parameters based on empirical data from previous papers: $\mu_\infty = 0.0035\,\mathrm{Pa\,s}$, $\mu_0 = 0.16\,\mathrm{Pa\,s}$, $\lambda = 8.2s$, $a = 0.64$, and $n = 0.2128$.[50] The behavior of the Carreau-Yasuda model for the range of shear rate values shown in Fig.22.

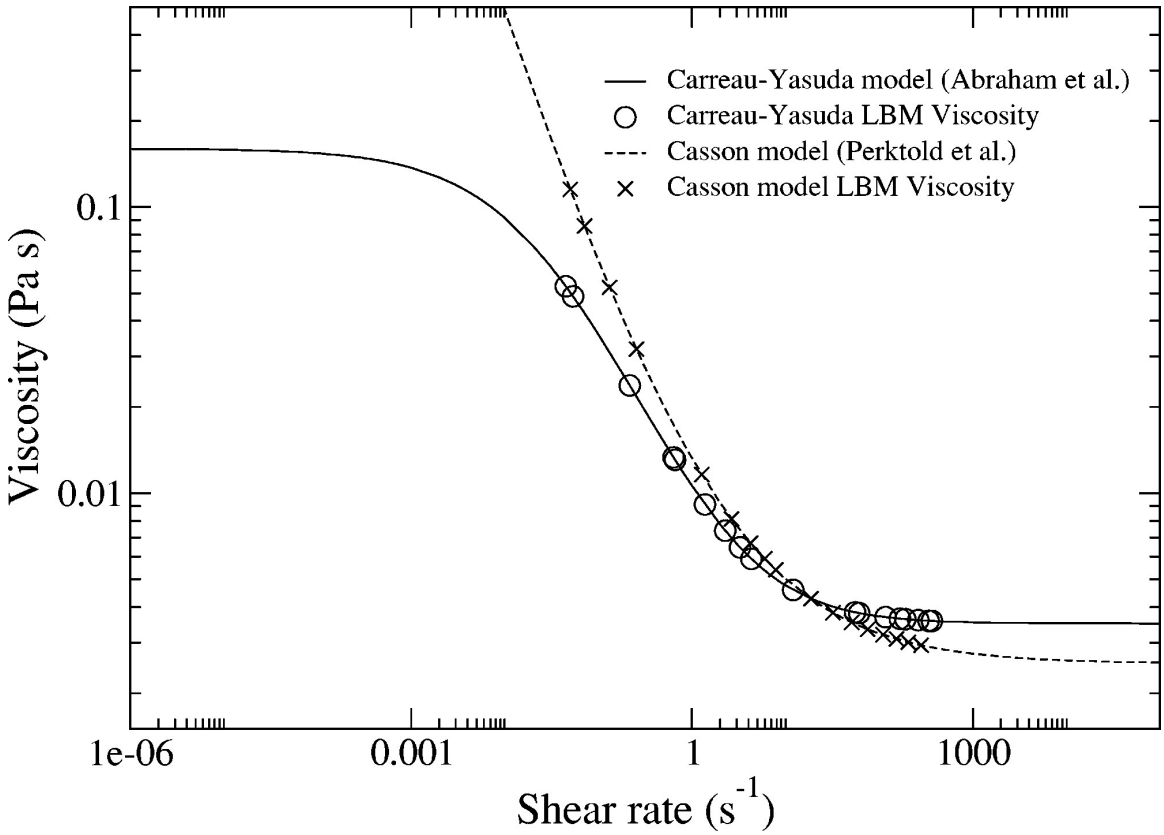


Figure 22: *The Carreau-Yasuda Model exhibits the power-law behavior between shear rates of* $0.001\,\mathrm{s}^{-1}$ *and* $1000\,\mathrm{s}^{-1}$ *and asymptotes to the* $\mu_0$ *and* $\mu_\infty$ *values at the extremes. The divergent behavior of the Casson model is observed as well.*[50]

.

The values defined above were all imported into ANSYS and pressure boundary conditions were specified. A simple block with a cross-section of 10 mm by 10 mm was imported and the permeability for the block was defined for each combination of porosities and pore diameters. Pore diameters were varied between 100-500 µm in increments of 100 µm. Porosities were varied between 70% - 90% in increments of 5%. Block thicknesses of 0.5 mm, 2 mm, and 5 mm were studied. The setup is illustrated in Fig.23.

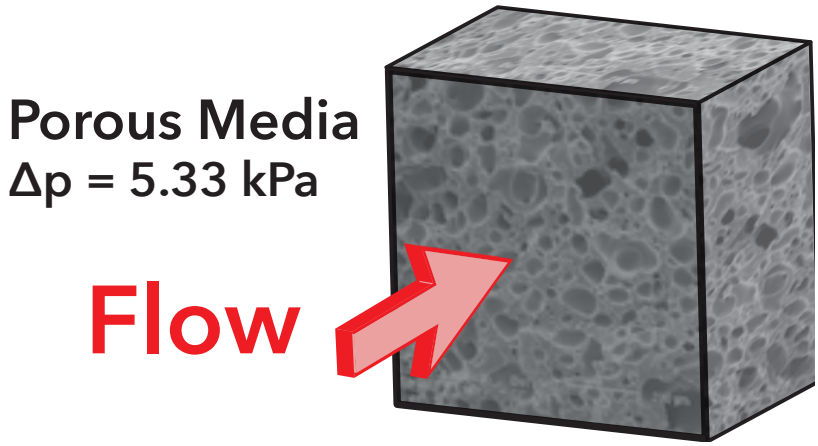


Figure 23: *The ANSYS model set up is made up of a block with the full thickness representing the porous region. The permeability of the porous region determines the velocity of blood through the block, in addition to the rest of the ANSYS momentum equations.*

# 3 Results

## 3.1 Fabrication of Silicone Rubbers

The fabrication method with silicone allows for creating of single and multiple layer cuffs of varying silicone materials. The size of the fabricated cuff can also be varied by scaling the molds in size, as shown in Fig.24.

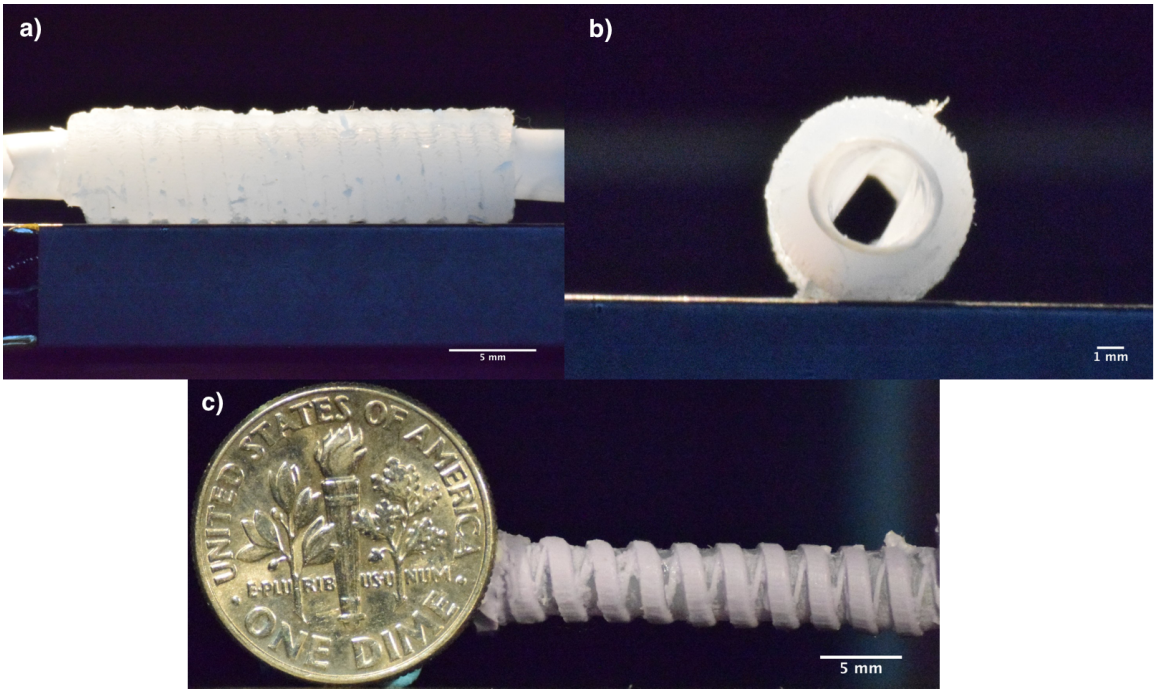


Figure 24: *Silicone rubber fabrication structures. a) The shunt,* 40 mm *in length, is grasped by a* 30 mm *cuff. The structure represents the full size of the shunt-cuff complex. The cuff is made of a single silicone rubber material (Eco-flex). b) The elliptical constriction at the cross section of the shunt is shown. c) The versatility of the method is presented. The cuff is scaled down by a factor of 2 in diameter. Multiple materials are introduced (Eco-flex and Oomoo) and an outer helical design is present.*

The geometry in Fig.24 satisfies the desired geometry of the cuff. The ends of the shunt remain fully circular and the transition to the elliptical constriction begins at the entrance of the cuff. The outer diameter remains at 4 mm and the internal

elliptical cross-section that reduces the area while maintaining the circumference with an x-axis length of 1.6 mm and y-axis length of 5.8 mm is present.

## 3.2 Injection Molding Results

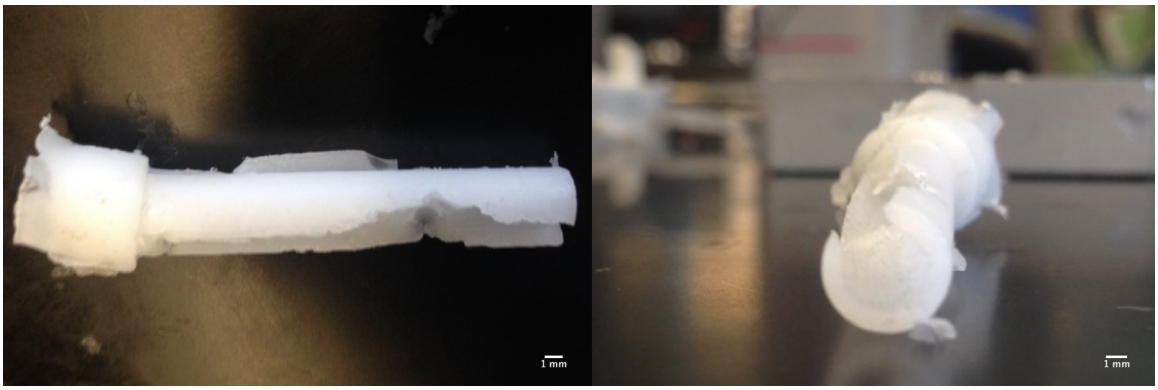


Figure 25: *Injection molding structures. The full size of resulting PCL structure (left) and the circular cross section (right) are presented. The full shape of the desired cuff did not form due to inability of melted PCL to penetrate through the mold. The formation of an elliptical constriction is visible but not completed. The cross section shows a homogeneous circular end with a gap PCL missing.*

The space between the constriction mold and the outer walls of the mold is too small and the highly viscous PCL was unable to be fully extruded into the gap. Additionally, the lower temperature of the mold leads to the solidification of PCL as it penetrates within, even with application of heating pads throughout the mold. Lastly, the side which PCL does not penetrate corresponds to the side on which centering rods are placed at the very top of the mold to center the constriction. The centering rods cause additional resistance to the flow of PCL on that specific side.

## 3.3 PCL "Jelly Roll" Technique

The "Jelly Roll" technique proved successful in creating homogeneous thin sheets of PCL in a simple and quick procedure with 500 µm, 250 µm, and 125 µm wires as spacers, as shown in Fig.28.

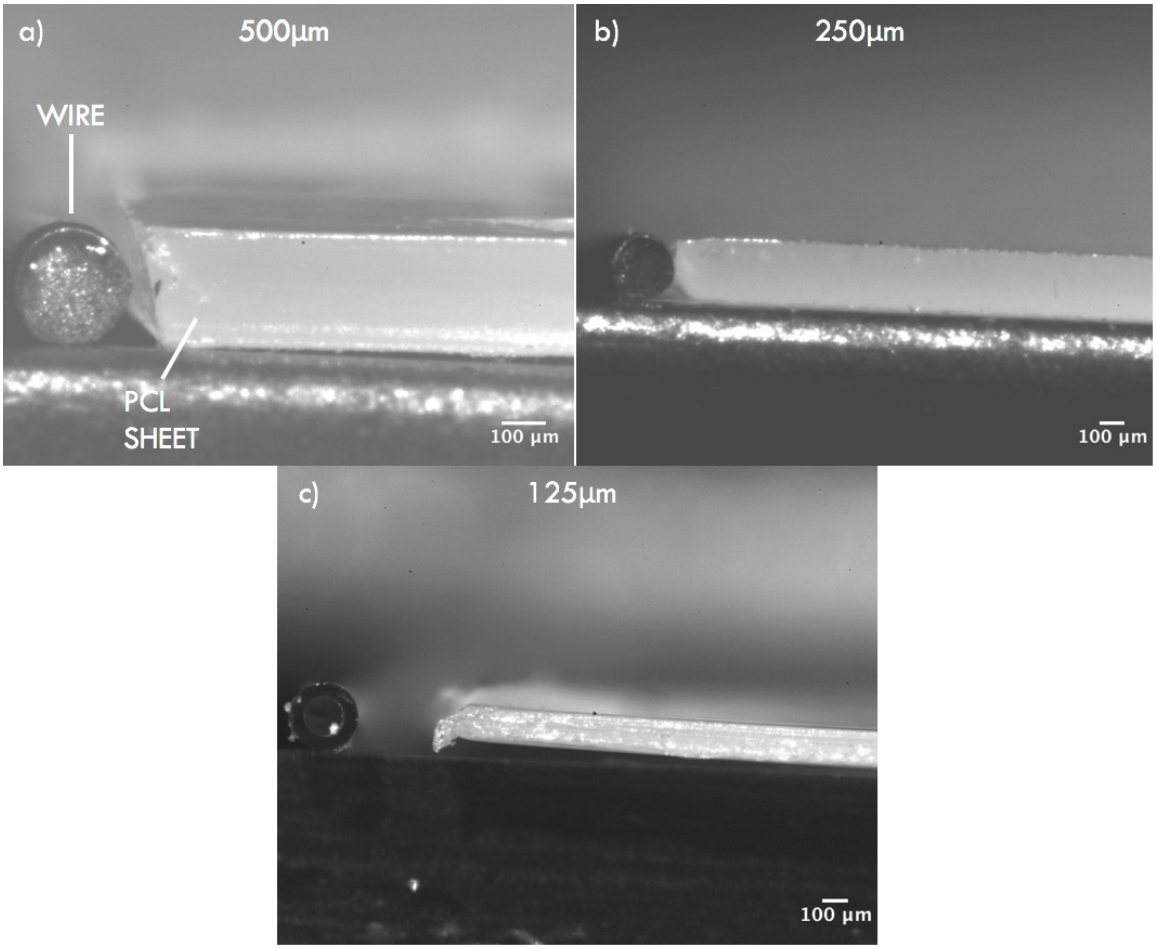


Figure 26: *Thin sheets of PCL. a) A* 500 µm *sheet of PCL with the wire that was utilized to fabricate the sheet beside it. b) A* 250 µm *sheet of PCL with wire beside it. c) A* 125 µm *sheet of PCL with a glass capillary beside it (wire used for fabrication). A camera (Fastcam mini UX100, Photron) combined with a long working-distance microscope (K-series, Infinity USA) was used to obtain these images.*

The sheets were then wrapped, by hand, around a 3D printed ABS elliptical mold with the same geometry as in Fig.14b. The wrapping was 3 layers thick and the layers were fused together by exposing the material to 60 °C temperatures. The wrapped structure and its close up is presented below.

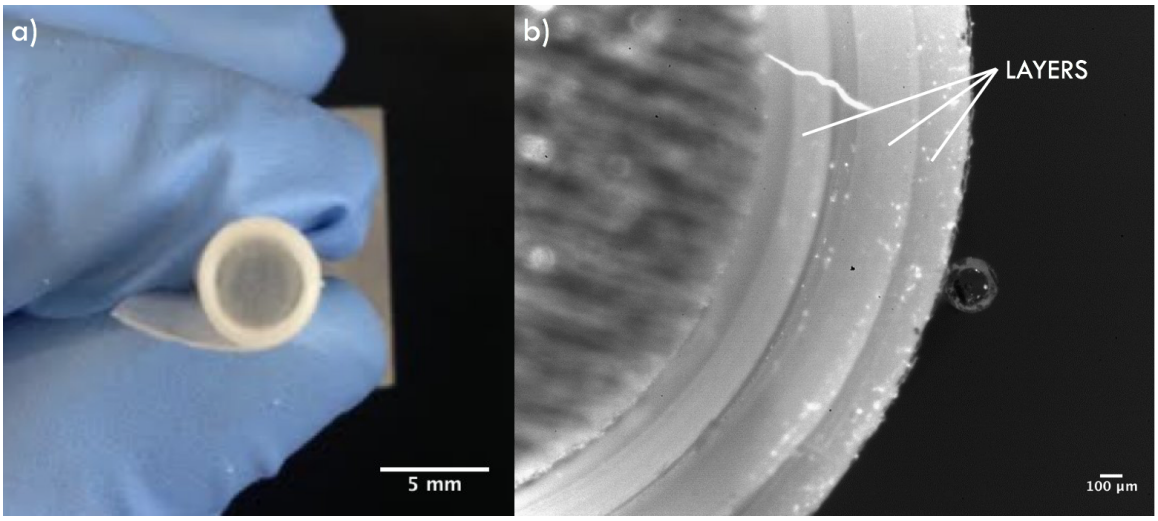


Figure 27: *Wrapped PCL sheet. a) Zoomed out image of wrapped PCL sheets around the desired elliptical mold. b) Close up image of wrapped PCL sheets with each layer tightly gripping the layer under it. The boundary between each layer can be transformed to a fused connection between layers by briefly heating the structure to the melting temperature of PCL.*

### 3.4 Effect of Cyclic Loading on Dissolution Rate

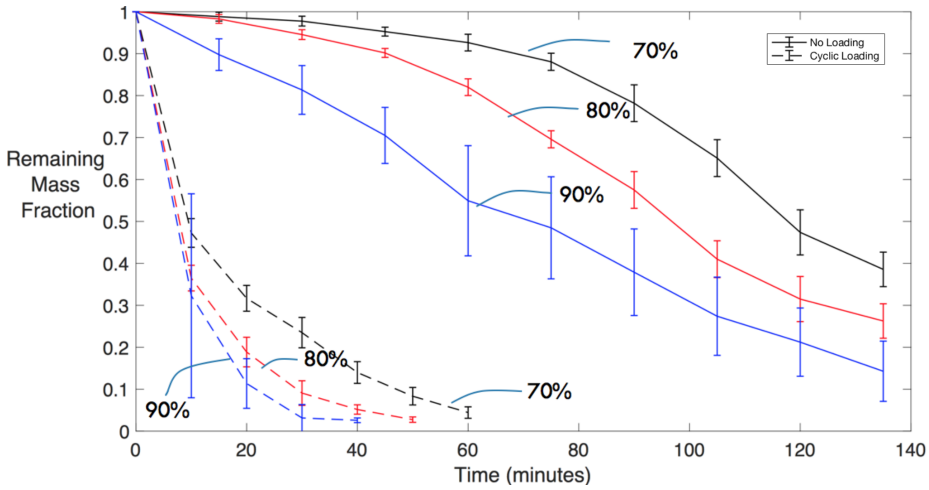


Figure 28: *PCL cyclic loading results. A total of 6 curves representing all tested conditions. The top 3 curves represent blocks without load application. The bottom 3 curves represent blocks exposed to cyclic loading. Each curve represents different porosities, from 70%to 90%.*

The degree to which blocks with no loading degraded at 135 min ranges between a mass fraction ratio of 0.39 at 70% to 0.14 at 90%. The dissolution profile for blocks without loading transitions to a nearly linear curve at a porosity of 90%. The PCL blocks under cyclic loading lose most of the block mass during the initial 10 min exposure.The dissolution time for blocks under cyclic loading decreases as porosity increases. The dissolution profile forming after the 10 min mark of blocks under cyclic loading suggests a decrease in dissolution rate over time. The variation in measurements is greater for 90% porous blocks in both loading and no loading cases.

### 3.5 Porous Flow Response

The Buckingham Pi theorem was implemented to incorporate the output parameters of the model, velocity and viscosity, into two dimensionless parameters. The non-dimensionalization was used to hopefully collapse all data points onto a single curve for convenient comparison to the theoretical solution. The following dimensionless parameters were defined.

$$\Pi_1 = \frac{L}{R} \tag{20}$$

and

$$\Pi_2 = \frac{u \cdot \mu}{\Delta P \cdot R}, \tag{21}$$

where $u$ is the flow velocity, $\Delta P$ is the pressure gradient across porous media, $L$ is the length of porous media, $R$ is the pore radius, and $\mu$ is viscosity

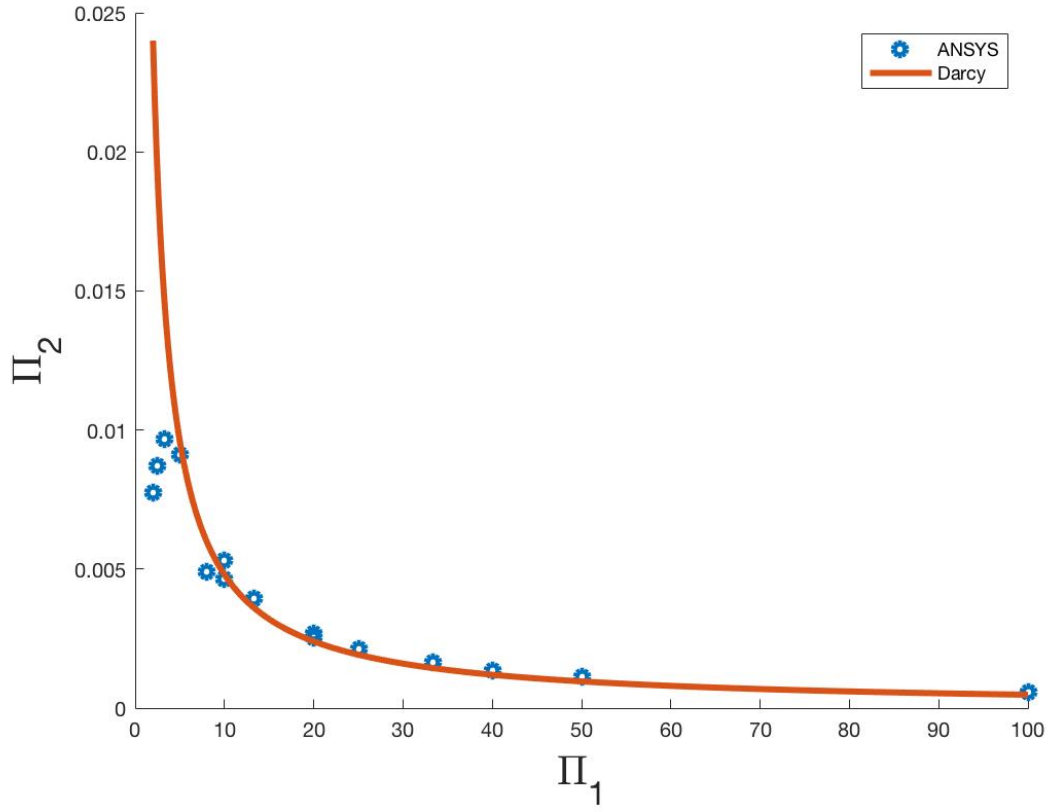


Figure 29: *Non-dimensionalized porous flow results for 80% porous PCL. The data points were collected as outputs from ANSYS and compared to the theoretical Darcy porous flow solution for the same conditions and geometry.*

The theoretical Darcy porous flow curve is developed from eqn.(14), not accounting for the momentum equations and the non-Newtonian behavior of blood that is included in the finite element simulation. The finite element analysis results closely follow the theoretical Darcy results following the initial 3 data points at low $\Pi_1$ values. Due to the shear-thinning behavior of blood, the viscosity is expected to increase as the thickness of the block is increased or as the radius of the block is decreased, both of which lead to lower flow velocity. The decrease in velocity leads to shear rates of decreased magnitude, allowing the blood to become more viscous. The general trend in the finite element methods' viscosity results is a decrease in

viscosity as $\Pi_1$ increases. The trend reverses at lower $\Pi_1$ values, leading to the discrepancy between the first 3 data points and the rest of the results. Only the 80% simulation result was plotted because porosity did not significantly influence the $\Pi_1$-$\Pi_2$ relationship.

# 4 Discussion

## 4.1 Fabrication Techniques

The attempted fabrication techniques provide multiple approaches to creating complex structures. The technique used to produce the silicone samples provided versatility when multiple layers of material are needed and when the size of the cuff needs to be changed. The transition to the injection molding technique with PCL proved difficult and did not result in the desired geometry. The technique can be improved by changing the centering method which will remove centering rods from the entrance point of the material into the mold. Further, the technique can be improved by creating larger spaces for PCL to flow through, as well as by heating the mold homogenously and to higher temperatures, maintaining PCL in melted form. The injection molding technique was not pursued further because the novel "jelly roll" technique provides more versatility, as well as better design resolution. The benefits of the "jelly roll" technique are presented below.

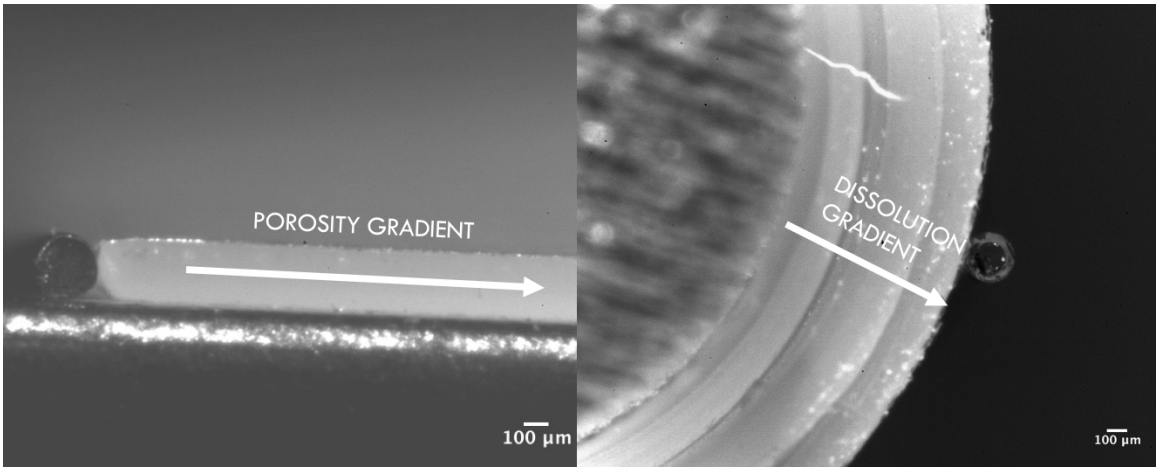


Figure 30: *Wrapped PCL sheet discussion. The figure represents the benefits of the "jelly roll" fabrication technique.*

The primary advantage of the "jelly roll" method is the ability to create virtually any geometry that can be achieved by the mold around which the PCL is

wrapped. The new limiting factor for geometry becomes the mold material as well as the fabrication process of the mold. The secondary advantage is the ability to create a porosity gradient along the length of the sheet. The PCL sheet can be increased in length, with higher porosity introduced at the beginning of the sheet and lower porosity introduced towards the end of the sheet. Wrapping the PCL sheet around the mold leads to the tertiary advantage of a dissolution gradient. Once wrapped, the higher porosity section of the sheet is on the inside, while the lower porosity section is towards the outside. Since dissolution of material is dependent on porosity, the material on the inside will dissolve at an accelerated rate compared to the outside, satisfying the need of the cuff to dissolve from the inside out and release the constriction.

## 4.2 Effect of Cyclic Loading on Dissolution Rate

It is important to note that the applied pressure on the PCL block applies compressive stress as opposed to the tensile characteristic of hoop stress that is applied in-vivo. Additionally, the viscoelastic behavior of PCL needs to be taken into account to relate the experimental frequency of 1 Hz to slight variations in heart rate in newborns, which is closer to 2 Hz. The compressive and tensile modulus of bulk PCL exhibits a 50 MPa difference, with introduction of porosity leading to almost identical values.[32] Additionally, the storage modulus and phase lag of PCL under cyclic loading has been found to be practically unchanged in the range of 1 Hz-10 Hz, completely enveloping the possible physiological heart rates.[51] Lastly, the applied stress is within the linear elastic region of PCL. The study reveals information on the effect of cyclic loading on dissolution as cyclic loading directly affects the flow of dissolving media through the block. Assuming a similar compressive and tensile elastic modulus, the change in pore size due to the applied stress is assumed identical. The results are applicable to higher frequencies due to

the limited change in viscoelastic properties of PCL at higher frequencies. The remaining difference between applying tensile and compressive stress is the increase in pore diameter experienced in tension, versus the decrease in pore diameter experienced in compression. For a more accurate representation of the mechanical effects, a setup that applies tensile stress instead of compressive stress used in this study will be needed. Figure 31 shows how the dissolution studies can be related to in-vivo conditions.

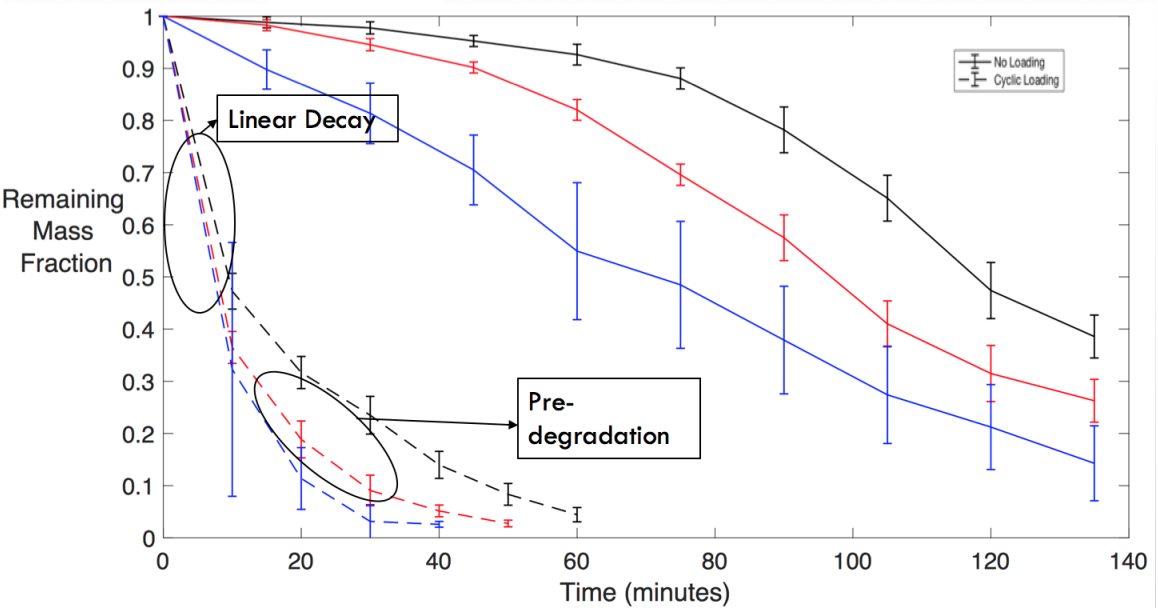


Figure 31: *PCL cyclic loading discussion. The dissolution profile drastically changes under cyclic loading. Additionally, the profile of the cyclically loaded blocks changes from a steep nearly linear dissolution to a more exponential decay behavior.*

The change observed between near linear decay and the exponential decay of the cyclically loaded blocks suggests that the applied force compacts the pores over time, preventing penetration of ethyl acetate into the structure and reducing the amount of surface area available for dissolution reactions. Another explanation is that a large amount of the polymer dissolves in the initial 10 min and there simply not enough polymer left to dissolve. If the two different dissolution profiles exist in degradation by blood, then the near linear decay portion can be used for a rapid

decay of material, while pre-degrading the PCL prior to implantation can be used if slower decay is desired.

### 4.3 Porous Flow Response

To better understand the behavior of porous flow results from ANSYS, the Reynolds number was calculated according the following equation.[52]

$$Re = \frac{\rho d_t u}{\mu} \tag{22}$$

where $Re$ is the Reynolds number, $\rho$ is the density, $d_t$ is the pore diameter, $u$ is the velocity, and $\mu$ is the viscosity.

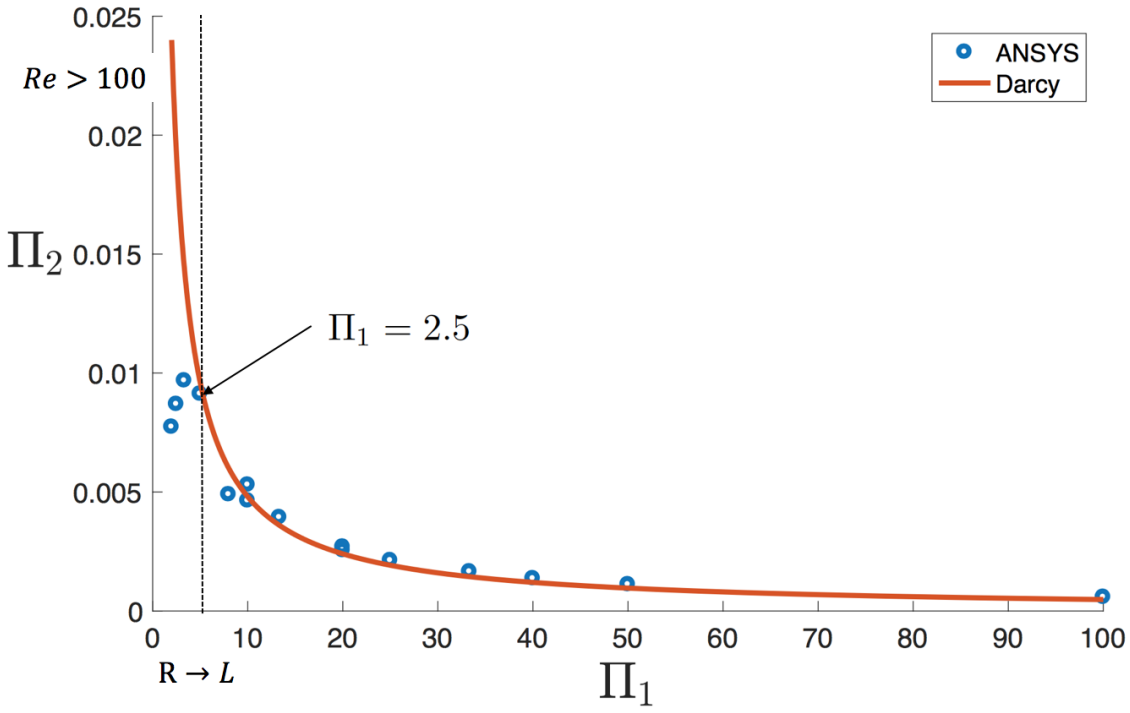


Figure 32: *Non-dimensionalized porous flow. The figure shows the point at which the discrepancy between ANSYS and the theoretical Darcy flow occurs.*

The Reynolds number was found to be above 100 at $\Pi_1 = 2.5$. According to Ma & Ruth et al.[52] the critical Reynolds number for which Darcy porous media

model diverges from the true solution is 13 making the point of discrepancy between finite element analysis and theoretical Darcy flow significantly outside of valid range. Additionally, as thickness of the block approaches the radius of the pore, the model loses its porous media properties and instead becomes a perforated plate with penetrating through holes. The results suggest that the finite element model is valid for certain thickness to radius ratios, allowing the model to be used for studying flow through the porous cuff for design parameters that satisfy $\Pi_1 > 2.5$.

# 5 Conclusions

The aim of the research was to address the mBT procedure cost, variability in sizing, frequent surgical intervention, and ability to prevent or at least monitor thrombosis. All four needs can be addressed through the design and fabrication of a cuff that will surround the shunt and provide gradual constriction release over time. The cuff will be designed to change in shape through dissolution in a gradual and controlled manner such that it "grows with the infant" with minimal surgical intervention. By implementing bioabsorbable materials to fabricate the cuff the size of the shunt constriction can be controlled through dissolution of the material in the body.

The development of a silicone rubber fabrication method allows for prototypes that will be used in animal testing to study the blood flow profile through the constriction and prevent thrombosis. The "jelly roll" fabrication technique provides a simple method for fabricating complex structures with biomaterials. The method can be combined with porosity to a dissolution gradient across the cuff thickness and lead to constriction release from within the shunt. The dissolution studies suggest the existence of two dissolution profiles, linear and parabolic, for porous PCL under cyclic loading. The profiles can be utilized in controlling the dissolution rate of PCL in vivo to achieve the gradual constriction release. Lastly, the developed ANSYS model will be utilized to study the effect of cuff geometry on flow through the porous material across the full cuff structure. The simulations will provide insight the relationship between pore diameter, porosity, and wall thickness with the dissolution rate of the cuff.

The presented research sets the initial steps for developing a sacrificial cardiopulmonary shunt cuff that allows for gradual blood flow increase in infants with CHD. The fabrication techniques, dissolution studies, and flow simulations will be improved to better achieve the design goals of the cuff.

# 6 References


[1] "What Are Congenital Heart Defects? - NHLBI, NIH". Nhlbi.Nih.Gov, 2017, https://www.nhlbi.nih.gov/health/health-topics/topics/chd.

[2] Dirks, V., Pretre, R., Knirsch, W., Valsangiacomo Buechel, E., Seifert, B., & Schweiger, M. (2013). Modified Blalock Taussig shunt: a not-so-simple palliative procedure. European Journal Of Cardio-Thoracic Surgery, 44(6), 1096-1102. http://dx.doi.org/10.1093/ejcts/ezt172

[3] "Congenital Heart Disease — Congenital Heart Defects — Medlineplus". Medlineplus.Gov https://medlineplus.gov/congenitalheartdefects.html.

[4] Arpagaus, M., Gray, D., Zierler, B. "Cardiac Catheterization In Children As Outpatients: Potential, Eligibility, Safety And Costs.". Pubmed, vol 13, no. 3, 2003, pp. 275-83. https://www.ncbi.nlm.nih.gov/pubmed/12903876.

[5] "Facts About Congenital Heart Defects — NCBDDD — CDC". Cdc.Gov https://www.cdc.gov/ncbddd/heartdefects/facts.html.

[6] Created by Wapcaplet in Sodipodi - Own work $https://commons.wikimedia.org/wiki/File:Diagram\_of\_the\_human\_heart\_(cropped).svg\#filelinks$

[7] The Cardiovascular System. 1st ed., Pearson Higher Education.

[8] van der Linde, D., Konings, E., Slager, M., Witsenburg, M., Helbing, W., Takkenberg, J., & Roos-Hesselink, J. (2011). Birth Prevalence of Congenital Heart Disease Worldwide. Journal Of The American College Of Cardiology, 58(21), 2241-2247. http://dx.doi.org/10.1016/j.jacc.2011.08.025

[9] "What Are Congenital Heart Defects? - NHLBI, NIH". Nhlbi.Nih.Gov https://www.nhlbi.nih.gov/health/health-topics/topics/chd.

[10] "Systemic To Pulmonary Artery Shunting For Palliation: Introduction And History, Palliative Surgery And Indications For A Shunt, Types Of Shunts". Emedicine.Medscape.Com, http://emedicine.medscape.com/article/905950-overview#a2.

[11] "Blalock-Taussig Shunt — Baby Heart". Babyheart.In, http://babyheart.in/tag/blalock-taussig-shunt/

[12] "BBC - GCSE Bitesize: Gore-Tex®". Bbc.Co.Uk.

[13] Jørgensen, C.S. and W.P. Paaske. "Physical And Mechanical Properties Of Eptfe Stretch Vascular Grafts Determined By Time-Resolved Scanning Acoustic Microscopy". European Journal Of Vascular And Endovascular Surgery, vol 15, no. 5, 1998, pp. 416-422. Elsevier BV, doi:10.1016/s1078-5884(98)80203-7.

[14] Catanese, J., Cooke, D., Maas, C., & Pruitt, L. (1999). Mechanical properties of medical grade expanded polytetrafluoroethylene: The effects of internodal distance, density, and displacement rate. Journal Of Biomedical Materials Research, 48(2), 187-192. http://dx.doi.org/10.1002/(sici)1097-4636(1999)48:2¡187::aid-jbm13¿3.0.co;2-m

[15] Dean, P., Hillman, D., McHugh, K., & Gutgesell, H. (2011). Inpatient Costs and Charges for Surgical Treatment of Hypoplastic Left Heart Syndrome. PEDIATRICS, 128(5), e1181-e1186. http://dx.doi.org/10.1542/peds.2010-3742

[16] Arpagaus, M., Gray, D., Zierler, B. "Cardiac Catheterization In Children As Outpatients: Potential, Eligibility, Safety And Costs". Cardiol Young, vol 13, 2003

[17] How Much Does Heart Surgery Cost? - Costhelper.Com". Costhelper, http://health.costhelper.com/heart-surgery.html.

[18] Chalom, R., Raphaely, R., & Costarino, A. (1999). Hospital costs of pediatric intensive care. Critical Care Medicine, 27(10), 2079-2085. http://dx.doi.org/10.1097/00003246-199910000-00001

[19] Alsoufi, B., Gillespie, S., Kogon, B., Schlosser, B., Sachdeva, R., & Kim, D. (2015). Results of Palliation With an Initial Modified Blalock-Taussig Shunt in Neonates With Single Ventricle Anomalies Associated With Restrictive Pulmonary Blood Flow. The Annals Of Thoracic Surgery, 99(5), 1639-1647. http://dx.doi.org/10.1016/j.athoracsur.2014.12.082

[20] Lincoln, J., Stark, J., Tynan, M., & Aberdeen, E. (1968). Constriction (banding) of Blalock–Taussig anastomosis for intractable congestive cardiac failure and pulmonary oedema. Thorax, 23(5), 524-529. http://dx.doi.org/10.1136/thx.23.5.524

[21] Schmid, F., Kampmann, C., Kuroczynski, W., Choi, Y., Knuf, M., Tzanova, I., & Oelert, H. (1999). Adjustable tourniquet to manipulate pulmonary blood flow after Norwood operations. The Annals Of Thoracic Surgery, 68(6), 2306-2309. http://dx.doi.org/10.1016/s0003-4975(99)00819-x

[22] Mizzi, J, and V Grech. "Acute Modified Blalock-Taussing Shunt Obstruction Successfully Treated with Urokinase and Heparin." Images in Paediatric Cardiology 7.3 (2005): 20–23. Print.

[23] By FrozenMan - Own work, CC BY-SA 4.0, https://commons.wikimedia.org/w/index.php?curid=36923196

[24] Nair, Lakshmi S., and Cato T. Laurencin. "Biodegradable Polymers As Biomaterials". Progress In Polymer Science, vol 32, no. 8-9, 2007, pp. 762-798. Elsevier BV, doi:10.1016/j.progpolymsci.2007.05.017.

[25] "Biomaterials- Evonik Health Care - Your Competitive Advantage". Resomer.Com, http://www.resomer.com/product/biodegradable-polymers/en/pharma-polymers/products/pages/bioresorbable-polymer.

[26] PLGA (Poly Lactic Co-Glycolic Acid) Uniform Dry Microspheres. 1st ed., Polysciences Inc., 2016, http://www.polysciences.com/skin/frontend/default/polysciences/pdf /TDS%20858.pdf.

[27] Gentile, P., Chiono, V., Carmagnola, I., & Hatton, P. (2014). An Overview of Poly(lactic-co-glycolic) Acid (PLGA)-Based Biomaterials for Bone Tissue Engineering. International Journal Of Molecular Sciences, 15(3), 3640-3659. http://dx.doi.org/10.3390/ijms15033640

[28] Göpferich, A. "Mechanisms Of Polymer Degradation And Erosion". Biomaterials, vol 17, no. 2, 1996, pp. 103-114. Elsevier BV, doi:10.1016/0142-9612(96)85755-3.

[29] Burkersroda, F., Schedl, L., & Göpferich, A. (2002). Why degradable polymers undergo surface erosion or bulk erosion. Biomaterials, 23(21), 4221-4231. http://dx.doi.org/10.1016/s0142-9612(02)00170-9

[30] Göpferich, Achim. "Polymer Bulk Erosion". Macromolecules, vol 30, no. 9, 1997, pp. 2598-2604. American Chemical Society (ACS), doi:10.1021/ma961627y.

[31] Yu, D., and A.J.C. Ladd. "A Numerical Simulation Method For Dissolution In Porous And Fractured Media". Journal Of Computational Physics, vol 229, no. 18, 2010, pp. 6450-6465. Elsevier BV, doi:10.1016/j.jcp.2010.05.005.

[32] Eshraghi, Shaun, and Suman Das. "Mechanical And Microstructural Properties Of Polycaprolactone Scaffolds With One-Dimensional, Two-Dimensional, And Three-Dimensional Orthogonally Oriented Porous Architectures Produced By Selective Laser Sintering". Acta Biomaterialia, vol 6, no. 7, 2010, pp. 2467-2476. Elsevier BV, doi:10.1016/j.actbio.2010.02.002.

[33] "Injection Molding Of Bioresorbable Polymer". $http://web.mit.edu/3.082/www/team1s/pres/Team_Template.pdf$

[34] "Injection Molding Of Polymers [Substech]". Substech.Com, $http://www.substech.com/dokuwiki/doku.php?id=injection\_molding\_of\_polymers$.

[35] Baker, S., Rohman, G., Southgate, J., & Cameron, N. (2009). The relationship between the mechanical properties and cell behaviour on PLGA and PCL scaffolds for bladder tissue engineering. Biomaterials, 30(7), 1321-1328. http://dx.doi.org/10.1016/j.biomaterials.2008.11.033

[36] Mooney, D., Baldwin, D., Suh, N., Vacanti, J., & Langer, R. (1996). Novel approach to fabricate porous sponges of poly(d,l-lactic-co-glycolic acid) without the use of organic solvents. Biomaterials, 17(14), 1417-1422. http://dx.doi.org/10.1016/0142-9612(96)87284-x

[37] Singh, L., Kumar, V., & Ratner, B. (2004). Generation of porous microcellular 85/15 poly (dl-lactide-co-glycolide) foams for biomedical applications. Biomaterials, 25(13), 2611-2617. http://dx.doi.org/10.1016/j.biomaterials.2003.09.040

[38] Sill, Travis J., and Horst A. von Recum. "Electrospinning: Applications In Drug Delivery And Tissue Engineering". Biomaterials, vol 29, no. 13, 2008, pp. 1989-2006. Elsevier BV, doi:10.1016/j.biomaterials.2008.01.011.

[39] Tay, B., Zhang, S., Myint, M., Ng, F., Chandrasekaran, M., & Tan, L. (2007). Processing of polycaprolactone porous structure for scaffold development. Journal Of Materials Processing Technology, 182(1-3), 117-121. http://dx.doi.org/10.1016/j.jmatprotec.2006.07.016

[40] Guarino, V., Causa, F., Ambrosio, L. "Porosity And Mechanical Properties Relationship In PCL Porous Scaffolds.". Applied Biomaterials Biomechanics, 2007, https://www.ncbi.nlm.nih.gov/pubmed/20799184.

[41] "Smooth-On Inc.". https://www.smooth-on.com.

[42] "Castaldo Plast-O-Wax Injection Wax". Riogrande.Com, https://www.riogrande.com/Product/Castaldo-Plast-O-Wax-Injection-Wax/7002005.

[43] Bok, M., Li, H., Yeo, L., & Friend, J. (2009). The dynamics of surface acoustic wave-driven scaffold cell seeding. Biotechnology And Bioengineering, 103(2), 387-401. http://dx.doi.org/10.1002/bit.22243

[44] Vital Signs in Children-Topic Overview. WebMD. from http://www.webmd.com/children/tc/vital-signs-in-children-topic-overview

[45] 17.5.4. Conservation Equations. Sharcnet.ca. from https://www.sharcnet.ca/Software/Ansys/16.2.3/en-us/help/flu_th/flu_th_sec_eulermp_theory_conseq.html

[46] 6.2.3. Porous Media Conditions. Sharcnet.ca. from https://www.sharcnet.ca/Software/Ansys/16.2.3/en-us/help/flu_ug/flu_ug_sec_bc_porous_media.html

[47] Retrieved from http://infohost.nmt.edu/ petro/faculty/Engler524/PET524-perm-2-ppt.pdf

[48] Wang, K., Liu, A., & Zhou, A. (2017). Theoretical analysis of influencing factors on resistance in the process of gas migration in coal seams. International Journal Of Mining Science And Technology, 27(2), 315-319. http://dx.doi.org/10.1016/j.ijmst.2017.01.011

[49] 7.3.5 Viscosity for Non-Newtonian Fluids. (2017). Jullio.pe.kr. from http://jullio.pe.kr/fluent6.1/help/html/ug/node297.htm

[50] Boyd, J., Buick, J., & Green, S. (2007). Analysis of the Casson and Carreau-Yasuda non-Newtonian blood models in steady and oscillatory flows using the lattice Boltzmann method. Physics Of Fluids, 19(9), 093103. http://dx.doi.org/10.1063/1.2772250

[51] Leung, L.,Naguib, H. (2012). Viscoelastic properties of poly(caprolactone) - hydroxyapatite micro- and nano-composites. Polymers For Advanced Technologies, 24(2), 144-150. http://dx.doi.org/10.1002/pat.3061

[52] Ma, H. & Ruth, D.W. Transp Porous Med (1993) 13: 139. doi:10.1007/BF00654407